ISSN 1674-1056
http://cpb.iphy.ac.cn
http://iopscience.iop.org/cpb
中国物理 B
Chinese Physics
中国物理 Chinese Physics B

Sm-Co high-temperature permanent magnet materials

Shiqiang Liu(刘世强)

Citation: Chin. Phys. B . 2019, 28(1): 017501. **doi:** 10.1088/1674-1056/28/1/017501
Journal homepage: http://cpb.iphy.ac.cn; http://iopscience.iop.org/cpb

What follows is a list of articles you may be interested in

Rare earth permanent magnets prepared by hot deformation process

Ren-Jie Chen(陈仁杰), Ze-Xuan Wang(王泽轩), Xu Tang(唐旭), Wen-Zong Yin(尹文宗), Chao-Xiang Jin(靳朝相), Jin-Yun Ju(剧锦云), Don Lee(李东), A-Ru Yan(闫阿儒)

Chin. Phys. B . 2018, 27(11): 117504. **doi:** 10.1088/1674-1056/27/11/117504

Mn-based permanent magnets

Jinbo Yang(杨金波), Wenyun Yang(杨文云), Zhuyin Shao(邵珠印), Dong Liang(梁栋), Hui Zhao(赵辉), Yuanhua Xia(夏元华), Yunbo Yang(杨云波)

Chin. Phys. B . 2018, 27(11): 117503. **doi:** 10.1088/1674-1056/27/11/117503

Nanocrystalline and nanocomposite permanent magnets by melt spinning technique

Chuanbing Rong(荣传兵), Baogen Shen(沈保根)

Chin. Phys. B . 2018, 27(11): 117502. **doi:** 10.1088/1674-1056/27/11/117502

Micromagnetism simulation on effects of soft phase size on $Nd_2Fe_{14}B/\alpha$–Fe nanocomposite magnet with soft phase imbedded in hard phase

Yu-Qing Li(李玉卿), Ming Yue(岳明), Yi Peng(彭懿), Hong-Guo Zhang(张红国)

Chin. Phys. B . 2018, 27(8): 087502. **doi:** 10.1088/1674-1056/27/8/087502

Improvement in coercivity,thermal stability,and corrosion resistance of sintered Nd-Fe-B magnets with $Dy_{80}Ga_{20}$ intergranular addition

Beibei Zhou(周贝贝), Xiangbin Li(李向斌), Xuejing Cao(曹学静), Gaolin Yan(严高林), Aru Yan(闫阿儒)

Chin. Phys. B . 2016, 25(11): 117504. **doi:** 10.1088/1674-1056/25/11/117504

TOPICAL REVIEW — Magnetism, magnetic materials, and interdisciplinary research

Sm–Co high-temperature permanent magnet materials

Shiqiang Liu(刘世强)†

240 *Jackson Ave., Braselton, GA* 30517, *USA*

(Received 29 November 2018; published online 25 December 2018)

Permanent magnets capable of reliably operating at high temperatures up to ∼ 450 °C are required in advanced power systems for future aircrafts, vehicles, and ships. Those operating temperatures are far beyond the capability of Nd–Fe–B magnets. Possessing high Curie temperature, Sm–Co based magnets are still very important because of their high-temperature capability, excellent thermal stability, and better corrosion resistance. The extensive research performed around the year 2000 resulted in a new class of $Sm_2(Co, Fe, Cu, Zr)_{17}$-type magnets capable of operating at high temperatures up to 550 °C. This paper gives a systematic review of the development of Sm–Co permanent magnets, from the crystal structures and phase diagrams to the intrinsic magnetic properties. An emphasis is placed on $Sm_2(Co, Fe, Cu, Zr)_{17}$-type magnets for operation at temperatures from 300 °C to 550 °C. The thermal stability issues, including instantaneous temperature coefficients of magnetic properties, are discussed in detail. The significance of nanograin structure, nanocrystalline, and nanocomposite Sm–Co magnet materials, and prospects of future rare-earth permanent magnets are also given.

Keywords: Sm–Co, $Sm_2(Co, Fe, Cu, Zr)_{17}$, high-temperature magnets, nanocomposite

PACS: 75.50.Ww, 75.50.–y **DOI:** 10.1088/1674-1056/28/1/017501

1. Introduction

Applications of Nd–Fe–B magnets have rapidly expanded since the mid-1980s. However, because of the low Curie temperature of $Nd_2Fe_{14}B$ compound (312 °C) and relatively low intrinsic coercivity, high-end Nd–Fe–B magnets can be used only around room temperature. Heavy rare earth, such as Dy and Tb, modification enhances the intrinsic coercivity to ∼ 2.4 MA/m, thus extending the operating temperature to ∼ 180 °C. Beyond that temperature, Nd–Fe–B magnets will be no longer appropriate for any dynamic applications.

Permanent magnet materials capable of reliably operating at high temperatures up to ∼ 450 °C are required in the advanced power systems of future aircraft, vehicles, and ships. A major objective of the advanced power systems is to increase device reliability, maintainability, and supportability. This advancement will be accomplished in part through the development of advanced power components such as magnetic bearings, integrated power units, and internal starter/generators for main propulsion engines. New high temperature magnets are enabling technologies for the development of these new power components. Power system designers frequently find that magnetic materials impose technological limitations on their designs. Compromises are generally required between the desired performance and the magnetic, mechanical, and electrical properties of available materials. If new materials can operate at > 300 °C, then new advanced designs will be possible. Air cooling, rather than complicated liquid cooling and its necessary logistics support, will become an operational capability. Likewise, oil-less/lube-less gas turbine engines and power systems will be possible.[1]

Possessing high Curie temperatures (727 °C for $SmCo_5$ and 920 °C for Sm_2Co_{17} compound), Sm–Co based magnets are still very important because of their high-temperature application capability, excellent thermal stability, and better corrosion resistance. The extensive research performed around the year 2000 resulted in a new class of $Sm_2(Co, Fe, Cu, Zr)_{17}$-type magnets capable of operating at high temperatures up to 550 °C.

Another important trend in rare earth permanent magnets research is nanocrystalline and hard/soft nanocomposite magnet materials. For conventional rare earth magnets, high uniaxial anisotropy is only a necessary condition for high coercivity, but not necessarily a sufficient condition for it. Often, compositional modification and specific heat treatment have to be imposed to develop useful coercivity, as in the case of $Sm_2(Co, Fe, Cu, Zr)_{17}$-type magnets. However, when the grain size is reduced from micrometer to nanometer range, a direct connection between magnetocrystalline anisotropy and intrinsic coercivity is established. This makes it possible to develop nanograin $Sm_2(Co, Fe)_{17}$ and nanocomposite $Sm_2(Co, Fe)_{17}$/Fe–Co magnets with significantly enhanced magnetization and Curie temperature, as a result of eliminating excessive Sm and completely getting rid of non-ferromagnetic Cu and Zr. The current status of research in this field will be briefly introduced, and the technical difficulties in making nanocomposite Sm–Co magnetic materials will be discussed.

In this paper, a detailed historical review of the development of Sm–Co permanent magnet materials is given and this

†Corresponding author. E-mail: eaaliu@yahoo.com

© 2019 Chinese Physical Society and IOP Publishing Ltd

development is compared with that of $Nd_2Fe_{14}B$-based magnets. Based on this comparison, prospects of future rare earth permanent magnet materials are given.

2. Historical review of development of Sm–Co permanent magnets

Prior to the development of Sm–Co permanent magnet materials the two important types of permanent magnets were so-called Alnico magnets and hard-magnetic ferrites. Alnico was invented in the early 1930s in Japan. It contained 24 wt.% Co, 14% Ni, 8% Al, 3% Cu, and 51% Fe (Alnico 5) and had a coercivity over 35 kA/m, or about double that of the best magnet steels. Since then, the properties of permanent magnets had been rapidly improved. The maximum energy product of Alnico 5 reached 40 kJ/m^3 in the 1940s and then 103 kJ/m^3 in the modified Alnico in the 1960s. The high coercivity in Alnico magnets was explained by shape anisotropy. The elongated strong ferromagnetic Fe–Co rich phase is embedded in a weak magnetic Al–Ni rich matrix, the shape anisotropy restricts the magnetization direction along the long axis of the Fe–Co phase, making demagnetization difficult.

During the years from 1933 to 1945, ferrites were developed into commercially useful materials. Hard-magnetic ferrites have the formula $MO{\cdot}6Fe_2O_3$ (where M = Ba or Sr). They have a hexagonal crystal structure and fairly large magnetocrystalline anisotropy, resulting in high coercivity. Hard ferrites exhibit greater coercive force (160–240 kA/m) but much lower remanence (0.25–0.35 T) and maximum energy product (12–28 kJ/m^3) than Alnico.

A major turning point for the development of permanent magnets occurred in the 1960s. In the period 1946–1952, the study of rare earth metals was greatly accelerated because of advances in chemical separation techniques that were developed in association with the Manhattan Project, 1942–1945. Methods for producing pure rare earth metals in quantity were developed which, in turn, stimulated interest in the use of rare earth metals as alloying additions.

In 1959, Nesbit[2] presented magnetic results for a series of Gd–Co alloys, which included the intermetallics $GdCo_2$, $GdCo_3$, and $GdCo_5$, and showed Gd and Co sublattices coupled antiparallel in each of these phases. This was followed in 1960 by the work of Hubbard[3] who observed in $GdCo_5$ a large coercive force of 637 kA/m, which he ascribed to the large magnetocrystalline anisotropy. The significance of this work was neglected, perhaps because Gd was expensive and the magnetization of $GdCo_5$ was rather low, and apparently it was not recognized that $GdCo_5$ was only one of a family of intermetallic compounds with potential for permanent magnet applications.

In 1966, Hoffer and Strant[4] reported that YCo_5 had an extremely large crystal anisotropy with a single easy axis of magnetization. The significance of this discovery was immediately recognized, and they suggested that YCo_5, and most other RCo_5 (R stands for rare earths) phases were potential candidate materials for new permanent magnets. Extensive studies followed to determine the permanent magnetic properties of the family of RCo_5 (1:5) compounds containing Y, Sm, Ce, La, Nd, Pr, and mischmetal (MM).[5–17] Out of these studies evolved a new generation of permanent magnet materials with outstanding properties, which feature a useful combination of high remanence and high coercivity.

Preliminary magnets made from YCo_5 by Strnat's group in 1966 had energy products of only about 8 kJ/m[34] and in 1967 the same group reported an energy product of 40.6 kJ/m^3 for $SmCo_5$.[5] Further improvements in energy product to 64.5 kJ/m^3 and then to 147.2 kJ/m^3 were reported in 1968 by Velge and Buschow[10,12] at Philips. The development of liquid-phase sintering techniques by Das[14] in 1969 and by Benz and Martin[16] in 1970 made fully dense and stable $SmCo_5$ magnets possible. The energy products reached by the latter methods ranged from 127 kJ/m^3 to 159 kJ/m^3 and culminated in the basic manufacturing technology for the first generation of commercial rare earth permanent magnets (REPM). Today, the best $(BH)_{max}$ of $SmCo_5$ is around 200 kJ/m^3. Partial substitution of Pr for Sm resulted in slightly enhanced magnetization and energy product.

The promise which the rare earth-cobalt intermetallic phases R_2Co_{17} (2:17) held as potential permanent magnets was recognized in the early 1970s. Basic properties such as saturation magnetization, Curie temperature, and crystallographic parameters of the binary compounds were studied in the mid-1960s at the US Air Force Materials Laboratory by Strnat's group.[18] From 1970 to 1973, Ray, Strant, Mildrum, and their co-workers[19–25] at the University of Dayton expanded the study to the quasi-binary $R_2(Co_{1-x}Fe_x)_{17}$ phases and systematically investigated the metallurgical and magnetic properties, including the magnetocrystalline anisotropy of these phases. The fact that 2:17 compounds, with or without Fe substitution, have substantially greater saturation magnetization values (1.2–1.6 T) led them to predict that a second generation of rare earth magnets with higher energy product was possible.[19–24]

However, the realization of practical 2:17 magnets proved more difficult. It was found that all the magnet fabrication methods that had worked well for $SmCo_5$, when applied to Sm_2Co_{17}, yielded only very low coercive force, usually less than 0.2 MA/m. Over a period of several years, many different experimental approaches were tried but no exciting results were obtained.

In 1974, Senno and Tawara[26] extended the range of $Sm(Co, Fe)_z$ to $z = 7.2$ by adding Cu, so that the alloys could be magnetically precipitation hardened. They obtained two-

phase sintered magnets in which the main phase has the 2:17 structure. Careful heat treatment made the coercivity in the 0.32–0.8 MA/m range. Later, Tawara and Senno[27] were able to obtain high coercivity in sintered $Sm(Co_{0.85}Fe_{0.05}Cu_{0.10})_8$. In 1976, Nagel[28] achieved energy products in excess of those for $SmCo_5$ in sintered magnets Sm(Co, Fe, Mn, Cr)$_{8.5}$. However, the Mn- and Cr-containing magnets had the severe disadvantage that its coercive force drops very quickly with increasing temperature above 20 °C.

An important breakthrough was made in 1977 when a group at TDK in Japan announced that the Fe content could be increased and the Co content lowered if these compositional changes were accompanied by a small addition of Zr or similar transition metals.[29,30] They obtained $B_r = 1.12$ T, $_MH_c = 0.6$ MA/m, and $(BH)_{max} = 240.3$ kJ/m^3 for an alloy corresponding to the nominal composition $Sm(Co_{0.674}Fe_{0.213}Cu_{0.100}Zr_{0.013})_{7.43}$. Further refinement of the isothermal aging and step aging heat treatment[31] and compositional adjustment[32] yielded a permanent magnet with $B_r = 1.2$ T, $_MH_c = 1$ MA/m, and $(BH)_{max} = 262.6$ kJ/m^3 for the nominal composition $Sm(Co_{0.65}Fe_{0.28}Cu_{0.05}Zr_{0.02})_{7.67}$. It is important to note that these magnets have a much better temperature coefficient of $_MH_c$ than the Mn- and Cr-containing magnets, making them much more useful for elevated-temperature applications. The 2:17 magnets, or the second generation rare earth permanent magnets, became commercially available in the early 1980s. The best magnetic properties of $(BH)_{max} = 271$ kJ/m^3, $B_r = 1.22$ T, $_MH_c = 1.35$ MA/m were obtained in $Sm(Co_{0.613}Fe_{0.316}Cu_{0.052}Zr_{0.019})_{7.88}$, a magnet containing low Sm, low Cu, and low Zr, but fairly high Fe.[33]

3. Phase diagram and crystal structures

Figure 1 shows the binary Sm–Co phase diagram.[34–36] There exist quite a few intermetallic compounds in the Sm–Co system, including Sm_2Co_{17}, $SmCo_5$, Sm_2Co_7, $SmCo_3$, $SmCo_2$, Sm_9Co_4, and Sm_3Co. Among them, $SmCo_5$ and Sm_2Co_{17} possess important technical significance. Sm_2Co_{17} is the most Co-rich compound, and it has a polymorphic phase transformation (α $Co_{17}Sm_2$ and β $Co_{17}Sm_2$ in Fig. 1) and has different crystal structures at high and low temperatures. In addition, Sm_2Co_{17} and $SmCo_5$ demonstrate finite homogeneity ranges, while others show as line compounds. The *R*–Co phase diagrams for other rare earths are generally similar, but with some minor systematic variations.

As shown in Fig. 2,[37] $SmCo_5$ has a hexagonal crystal structure (1:5 H, space group: $P6/mmm$; prototype: $CaCu_5$), while Sm_2Co_{17} has a rhombohedral crystal structure (2:17 R, space group: $R\bar{3}m$; prototype: Th_2Zn_{17}) at room temperature and a hexagonal crystal structure (2:17 H, space group: $P6_3/mmc$; prototype: Th_2Ni_{17}) at high temperatures (1300–1340 °C). The common characteristic of all these three crystal structures is that their *c*-axes are the unique easy magnetization directions. This uniaxial anisotropy is the basis for $SmCo_5$ and Sm_2Co_{17} to become high-performance permanent magnets.

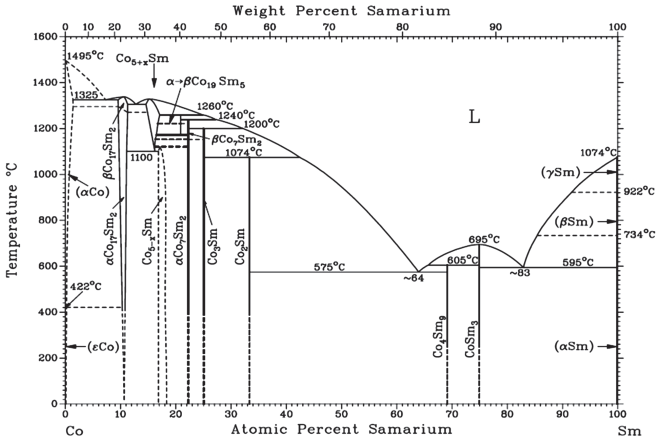


Fig. 1. Binary Co–Sm equilibrium phase diagram.[34–36]

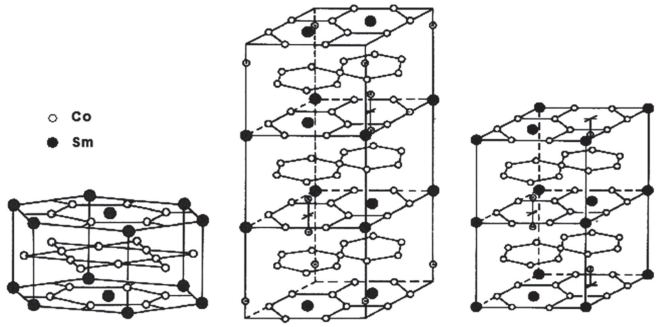


Fig. 2. Crystal structures of (a) $SmCo_5$ (1:5 H), (b) Sm_2Co_{17} (2:17 R), and (c) Sm_2Co_{17} (2:17 H).[37]

4. Intrinsic magnetic properties of *R*–Co compounds

Three important prerequisites for high-performance permanent magnet materials are high saturation magnetization, high Curie temperature, and high uniaxial magnetocrystalline anisotropy. Saturation magnetization and Curie temperature values of the *R*–Co binary systems are illustrated in Figs. 3 and 4, respectively. As a general rule for the 4f–3d exchange interaction, the light rare earths couple parallel with Co, yielding high saturation magnetization, while the heavy rare earths couple antiparallel with Co, resulting in low saturation magnetization.

Figure 5 shows anisotropy field H_a for binary RCo_5 compounds with R = Y, La, Ce, Pr, Nd, Sm, and MM. It is obvious that $SmCo_5$ compound has the highest anisotropy field. Figure 6 shows anisotropy field H_a for binary R_2Co_{17} compounds with R = Y, Ce, Pr, Nd, and Sm. It is obvious that among all 2:17 compounds, only Sm_2Co_{17} has uniaxial magnetocrystalline anisotropy and possesses a moderately large crystalline

anisotropy field.

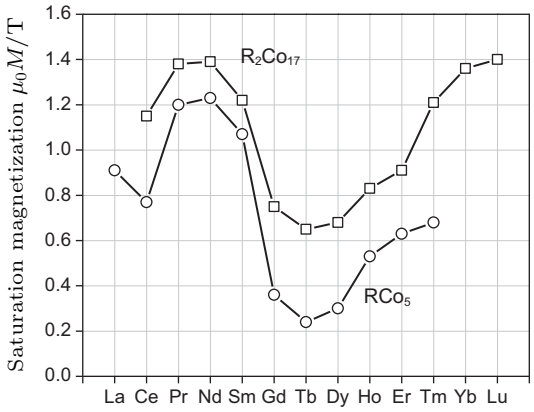


Fig. 3. Room-temperature saturation magnetization values of $R\mathrm{Co}_5$ and $R_2\mathrm{Co}_{17}$ compounds.

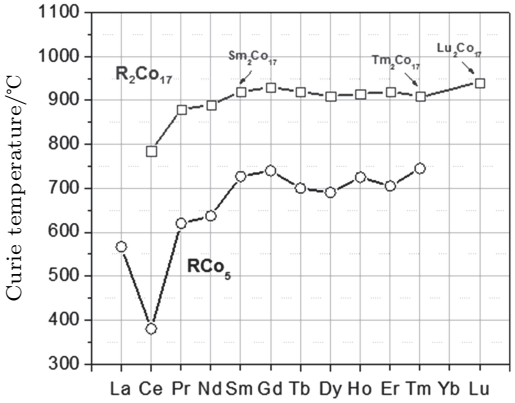


Fig. 4. Curie temperatures of $R\mathrm{Co}_5$ and $R_2\mathrm{Co}_{17}$ compounds.

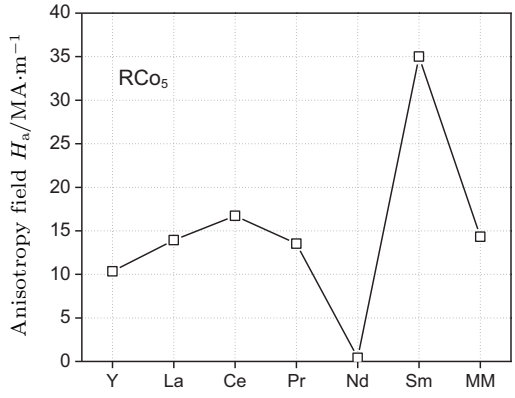


Fig. 5. Anisotropy field H_a for binary $R\mathrm{Co}_5$ compounds.

It is well known that for a rare earth–transition metal (RE–TM) compound, Curie temperature is primarily determined by the TM sublattice, while crystalline anisotropy is primarily contributed by the RE sublattice unless at temperatures close to the Curie point. Research on RE–TM compounds indicates that among all 3d transition metals, Co provides the highest Curie temperature, while among all light rare earths, Sm usually provides the highest crystalline anisotropy. One exception is the cubic Laves 1:2 compounds for which the Fe compounds have higher Curie temperature than the Co compounds.

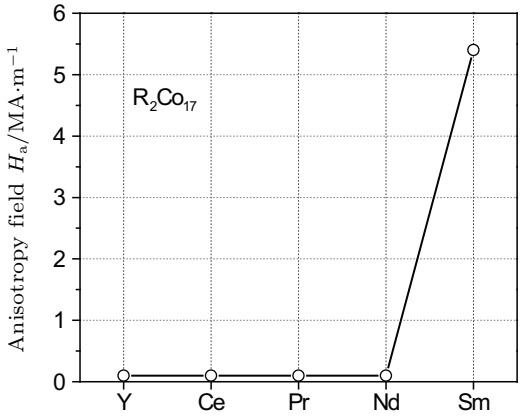


Fig. 6. Anisotropy field H_a for binary $R_2\mathrm{Co}_{17}$ compounds.

Figure 7 shows Curie temperature T_C versus Co content for Sm–Co binary compounds. In this figure, Curie temperature data for LaCo_{13} and $\mathrm{Sm}_2\mathrm{Co}_{14}\mathrm{B}$ are also included. It can be seen from Fig. 7 that there exists a linear relationship between Curie temperatures and the Co content, which clearly demonstrates the importance of the Co content to Curie temperature. Similarly, there exists a linear relationship between saturation magnetization and the Co content, as shown in Fig. 8.

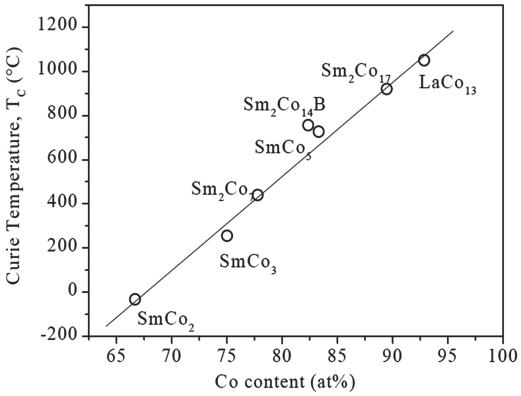


Fig. 7. Curie temperature T_C versus Co content for Sm–Co binary compounds. Data for LaCo_{13} and $\mathrm{Sm}_2\mathrm{Co}_{14}\mathrm{B}$ are also included.

Table 1 lists the intrinsic properties of some *R*–Co compounds. It is shown that among all light rare earth-Co compounds, SmCo_5 possesses the highest magnetocrystalline anisotropy, while $\mathrm{Sm}_2\mathrm{Co}_{17}$ combines high saturation magnetization, high Curie temperature, and moderately high anisotropy. As for heavy rare earth–Co compounds, HRCo_5 and $\mathrm{HR}_2\mathrm{Co}_{17}$ (with HR = Gd, Tb, and Dy) have low saturation magnetization, while $\mathrm{Tm}_2\mathrm{Co}_{17}$, $\mathrm{Yb}_2\mathrm{Co}_{17}$, and $\mathrm{Lu}_2\mathrm{Co}_{17}$ have fairly high saturation magnetization, but with unfavorable magnetocrystalline anisotropy, except for $\mathrm{Tm}_2\mathrm{Co}_{17}$, which shows uniaxial anisotropy, but its anisotropy field is not high.

A small amount of Fe substitution for Co in Tm_2Co_{17} slightly increases its anisotropy field. For Yb_2Co_{17} and Lu_2Co_{17}, a small amount of Fe substitution for Co changes the anisotropy from easy-basal-plane to uniaxial, though the anisotropy fields are not high in both cases.

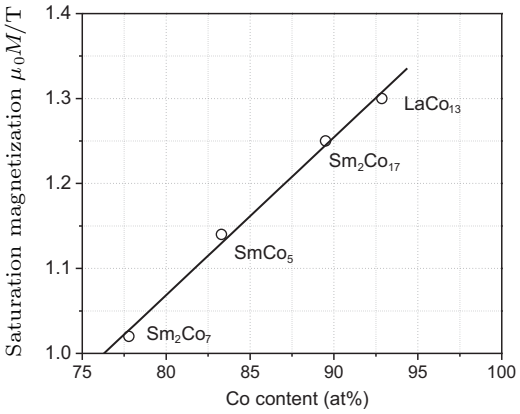


Fig. 8. Saturation magnetization versus Co content for Sm–Co binary compounds. Date for $LaCo_{13}$ is also included.

5. Sm–Co permanent magnets capable of operating up to 300 °C

Sm–Co permanent magnets are based on $SmCo_5$ and Sm_2Co_{17} compounds. The composition of a $SmCo_5$ magnet is slightly Sm rich, as compared with its chemical stoichiometry. Its microstructure is basically a featureless single phase, while a small amount of oxide particles and sometimes a minor Sm_2Co_7 phase can also exist. It is a generally accepted idea that the coercivity of $SmCo_5$ magnet is determined by nucleation field, though it is believed that grain boundary pinning may also play an important role.

On the other hand, the composition and microstructure of Sm_2Co_{17}-based magnets are more complicated. As mentioned in Section 2, in order to develop useful coercivity, extra Sm is required and considerable amounts of Cu and Zr have to be added into the alloy. In addition, a complex and long-term heat treatment procedure must be employed (the detailed heat treatment procedure is given in Section 8). Figure 9 shows a TEM microstructure of a typical $Sm_2(Co, Fe, Cu, Zr)_{17}$-type magnet.[40] Sintered 2:17 magnets have grains of micrometers in size, with a fine, nanometer cellular structure within each grain. As shown in Fig. 9, the cellular structure consists of three coherent phases: a 2:17 cell interior phase; a 1:5 cell boundary phase rich in Sm and Cu; and a platelet phase rich in Zr. It is believed that the domain wall pinning in the 1:5 cell boundary phase is the origin of high coercivity.

Table 1. Intrinsic properties of some *R*–Co compounds at room temperature.

Compound	$\mu_0 M_s$/T	T_C/K	K_1/MJ·m^{-3}	H_a/MA·m^{-1}	Anisotropy type	Ref.
YCo_5	1.06	987	6.5	10.3	uniaxial	[37], [38]
$LaCo_5$	0.91	840	6.3	13.9	uniaxial	[37]
$CeCo_5$	0.77	653	6.4	16.7	uniaxial	[37]
$PrCo_5$	1.20	893	8.1	13.5	uniaxial	[37]
$NdCo_5$	1.23	910	0.7	0.4	easy basal plane	[37], [38]
$SmCo_5$	1.10	1020	17.2	~ 35	uniaxial	[37]–[39]
$GdCo_5$	0.18	1008	4.6	~ 21	uniaxial	[37]
$TbCo_5$	0.24	973		0.5	easy basal plane	[37]
$DyCo_5$	0.30	966		2.0	uniaxial	[37]
$HoCo_5$	0.53	992			uniaxial	[37]
$ErCo_5$	0.64	978	4.5	8.0	uniaxial	[37]
$TmCo_5$	0.67	1012			uniaxial	[37]
Y_2Co_{17}	1.25	1167	–0.34		easy basal plane	[37], [38]
Ce_2Co_{17}	1.15	1053		1.2	easy basal plane	[37]
Pr_2Co_{17}	1.38	1153	–0.6		easy basal plane	[37]
Nd_2Co_{17}	1.39	1150	–1.1		easy basal plane	[37], [38]
Sm_2Co_{17}	1.22	1190	3.3	5.4	uniaxial	[37]–[39]
$Sm_2(Co_{0.7}Fe_{0.3})_{17}$	1.45	1113	3.0	4.1	uniaxial	[37]
Gd_2Co_{17}	0.75	1193	–0.5		easy basal plane	[37]
Tb_2Co_{17}	0.66	1188	–3.2		easy basal plane	[37], [90]
Dy_2Co_{17}	0.68	1152	–2.6		easy basal plane	[37], [38]
Ho_2Co_{17}	0.84	1155	–0.9		easy basal plane	[37], [90]
Er_2Co_{17}	0.91	1186	0.72	2.5	uniaxial	[37], [38], [92]
Tm_2Co_{17}	1.21	1180	0.56	2.6	uniaxial	[37], [91]
$Tm_2(Co_{0.82}Fe_{0.18})_{17}$	1.42	1153		3.0	uniaxial	[41], [42], [91]
Yb_2Co_{17}	1.36				easy basal plane	[37]
Lu_2Co_{17}	1.40	1203		0.9	easy basal plane	[37], [91]
$Lu_2(Co_{0.85}Fe_{0.15})_{17}$				2.1	uniaxial	[91]

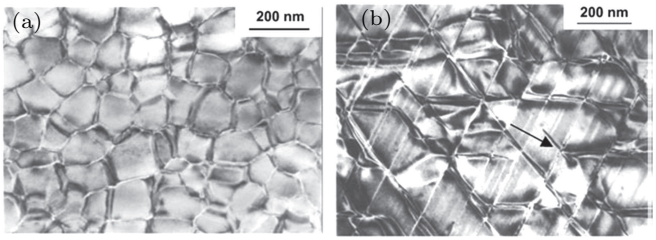


Fig. 9. TEM micrographs of a sintered $Sm_2(Co, Fe, Cu, Zr)_{17}$-type magnet. (a) Section perpendicular to the alignment direction; (b) section parallel to the alignment direction. Arrow (→) in panel (b) is the alignment direction (*c*-axis).[40]

Demagnetization curves of commercial $SmCo_5$ and $Sm_2(Co, Fe, Cu, Zr)_{17}$-type magnets at various temperatures are shown in Figs. 10 and 11 (By courtesy of Electron Energy Corporation). Both types of magnets can be used up to 300 °C.

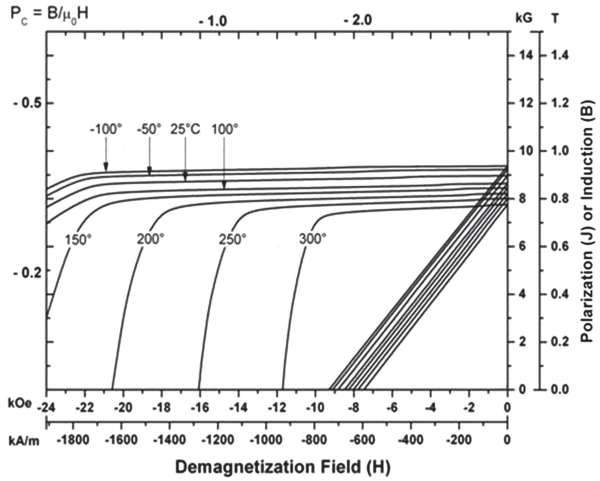


Fig. 10. Demagnetization curves of commercial $SmCo_5$ magnets.

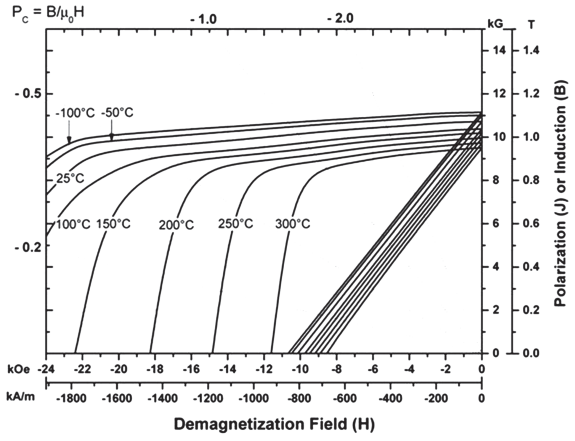


Fig. 11. Demagnetization curves of commercial Sm_2TM_{17} magnets.

Permanent magnets with very low temperature coefficients of magnetization over a wide temperature range are required for many applications. Examples are microwave tubes, gyros, accelerometers, and conventional moving-coil meters. The flux provided by most permanent magnets decreases on heating. This is an intrinsic property for all ferromagnetic materials, in which the magnetization will eventually drop to zero at their Curie temperatures. On the other hand, for most heavy rare earth–Co compounds, for example, $GdCo_5$ and Gd_2Co_{17}, the magnetization increases when temperature enhances before reaching a peak value. Based on this characteristic, partial substitution of heavy rare earth, such as Gd, for Sm can be made to form temperature-compensated (Sm,Gd)–Co magnets which may show a near zero temperature coefficient of magnetization from −50 °C to about 150 °C with a peak magnetization at around room temperature. Demagnetization curves of commercial temperature-compensated $(Sm,Gd)Co_5$ and $(Sm,Gd)_2(Co, Fe, Cu, Zr)_{17}$-type magnets at various temperatures are shown in Figs. 12 and 13 (By courtesy of Electron Energy Corporation). Both types of temperature-compensated magnets can be used up to 300 °C.

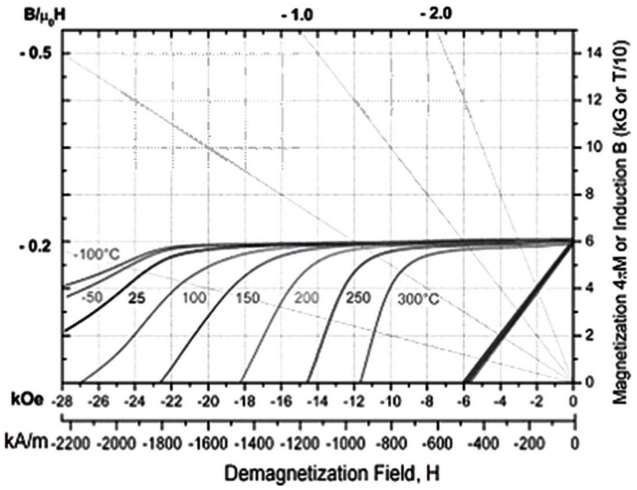


Fig. 12. Demagnetization curves of $(Sm,Gd)Co_5$ magnets.

It is obvious from Fig. 3 that Tm_2Co_{17}, Yb_2Co_{17}, and Lu_2Co_{17} have much higher magnetization than Gd_2Co_{17}. Figure 14 compares temperature dependence of magnetization for Sm_2TM_{17} and $Tm_2(Co, Fe)_{17}$. If Tm, Yb, or Lu can be incorporated into temperature-compensated (Sm,Gd)–Co magnets, then improved magnetic performance could be expected. However, because R_2Co_{17} (R = Tm, Yb, Lu) have poor anisotropy, developing enough high coercivity would be a technical challenge.

Powder metallurgy is used to manufacture commercial Sm–Co magnets. Its processing procedures include vacuum melting, ingot crushing, ball or jet milling, powder magnetic alignment, compaction, sintering, and heat treatment. Alternatively, Sm–Co alloy powders can be produced by a reduction-diffusion process using Sm_2O_3, Co powder, and Ca or CaH_2 as a reduction agent.

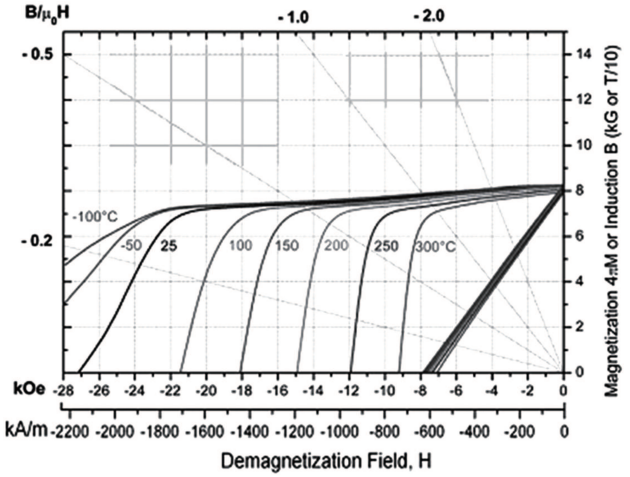


Fig. 13. Demagnetization curves of $(Sm,Gd)_2TM_{17}$-type magnets.

Sintered Sm–Co magnets are very hard and brittle, therefore machining them into the final shape and size is often troublesome, especially for tiny magnetic parts. This led to the development of bonded Sm–Co magnets,[37] which are made by consolidating a magnet powder with a polymer matrix. Thermosetting binders, such as epoxy resin, are employed in compression-molded magnets, while thermoplastic binders, like nylon, are used for injection-molded magnets, and elastomers, such as rubber, for extruded magnets.[43] Table 2 lists the magnetic properties of some Sm–Co magnets.

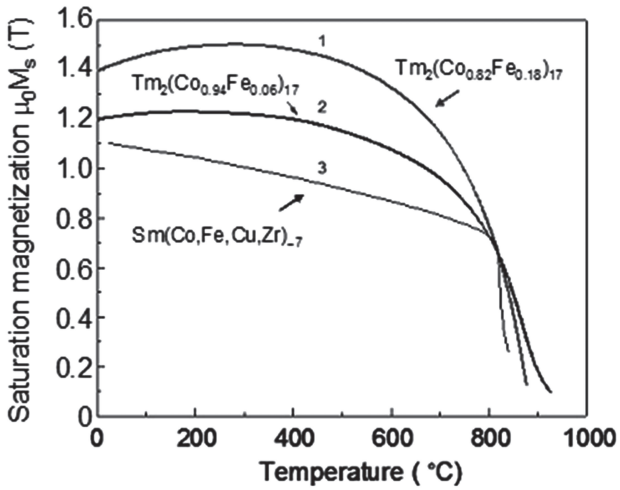


Fig. 14. Saturation magnetization versus temperature for $Tm_2(Co_{0.82}Fe_{0.18})_{17}$, $Tm_2(Co_{0.94}Fe_{0.06})_{17}$,[41,42] and Sm(Co, Fe, Cu, Zr)$_{\sim 7}$.

Table 2. Magnetic properties of some commercial Sm–Co magnets (TM stands for Co, Fe, Cu, and Zr).

Magnets	$\mu_0 M_r$/T	${}_MH_c$/kA·m^{-1}	${}_BH_c$/kA·m^{-1}	$(BH)_{max}$/kJ·m^{-3}
$SmCo_5$, $(Sm,Pr)Co_5$	0.8–0.96	> 1900	635–740	135–190
Sm_2TM_{17}	1.0–1.2	> 1900	710–840	180–255
Temp. compensated $(Sm,Gd)Co_5$	0.5–0.75	> 1900	400–600	64–120
Temp. compensated $(Sm,Gd)_2TM_{17}$	0.8–0.95	> 1900	480–720	80–175
Bonded $SmCo_5$	0.4–0.5	600–1600	240–520	32–65
Bonded Sm_2TM_{17}	0.6–0.8	400–1600	310–520	64–130

6. High-temperature $Sm_2(Co, Fe, Cu, Zr)_{17}$-type magnets capable of operating up to 550 °C

Possessing the highest Curie temperature and moderately high magnetization and energy product among high-performance rare earth permanent magnets, Sm_2TM_{17} magnets are the best conventional high-temperature permanent magnets.[44,45] A conventional Sm_2TM_{17} magnet can operate at up to 300 °C. The problem associated with higher temperature (> 300 °C) operation is that the intrinsic coercivity (${}_MH_c$) of these magnets drops sharply with increasing temperature. Upon heating, ${}_MH_c$ of the 2:17 magnets drops sharply from their room temperature values of 1.5–2.5 MA/m (or higher) to only 0.2–0.5 MA/m at 400 °C and 0.1–0.2 MA/m at 500 °C. Low intrinsic coercivity at high temperatures results in a nonlinear 2nd quadrant induction demagnetization curve (*B* curve) above ~ 300 °C. A linear 2nd quadrant *B* curve is critical for all dynamic applications, such as for generators, motors, and actuators.

In a dynamic application, the operating point of a magnet keeps cycling on the *B* curve. If the intrinsic coercivity is low, then the *B* curve can be nonlinear and a knee appears. Under this circumstance, the operating point of the magnet can be reduced to below the knee in the *B* curve and the induction can be significantly reduced irreversibly. If the intrinsic coercivity of a magnet is sufficiently high, then the *B* curve will be linear and the induction will be reversible around the operating point even at a quite low permeance value as shown in Fig. 15. The maximum operating temperature of a magnet (T_{max}) can be defined as the temperature limit at which the *B* curve of the magnet still maintains linearity. Therefore, to increase the operating temperature of permanent magnet materials, the key is to increase their intrinsic coercivity at high temperatures, so that their induction demagnetization curves remain linear at the operating temperature.

Around the year 2000, extensive research was carried out to substantially improve the high-temperature performance of Sm_2TM_{17}-type permanent magnets. As a result of that effort, the maximum operating temperature of permanent magnets was increased from around 300 °C to as high as 550 °C. This advance was made on systematic studies of the effects

of compositions on high-temperature intrinsic coercivity of Sm_2TM_{17}-type of permanent magnets.

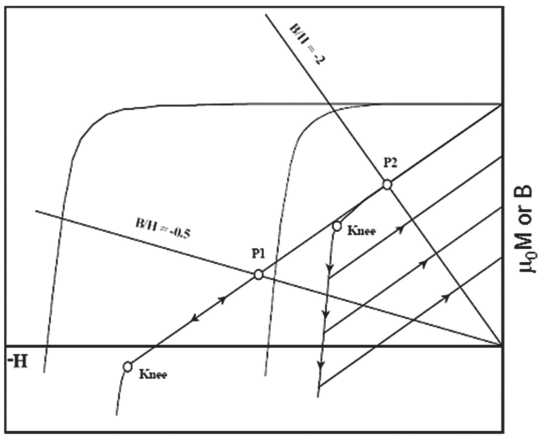


Fig. 15. Intrinsic coercivity and linearity of an induction demagnetization curve.

6.1. Effects of compositions on high-temperature intrinsic coercivity of Sm–TM permanent magnets

Compositions play a critical role in determining coercivity of Sm_2TM_{17}-type magnets. It is important to realize, however, that (i) the effect of an element on coercivity may be different at room temperature from what it is at elevated temperatures — this is especially true for Fe and Sm; (ii) the enhancement of an element on coercivity may have a peak value, and the optimal content corresponding to the peak coercivity is often different at different temperatures; (iii) there exist interactions among different alloy components. All these factors make the effects of compositions on coercivity very complicated.

Fe is an important element for substituting Co in binary R_2Co_{17} compounds. Fe substitution for Co always enhances magnetization, but decreases Curie temperature. The effect of Fe substitution on crystalline anisotropy of R_2Co_{17} is usually favorable at least around room temperature. R_2Co_{17} (R = Ce, Pr, Gd, Yb, Lu, and Y) demonstrate unfavorable easy-basal-plane anisotropy. However, substitution of an appropriate amount of Fe for Co changes the anisotropy to uniaxial. On the other hand, R_2Co_{17} (R = Sm, Er, and Tm) demonstrate uniaxial anisotropy and this anisotropy remains up to around 50–60 at.% Fe substitution.

Increasing Fe content in $Sm_2(Co, Fe, Cu, Zr)_{17}$-type magnets effectively enhances magnetization and leads to higher energy product. It also increases the room temperature intrinsic coercivity before a peak value is reached. However, high Fe content results in significantly low coercivity at elevated temperatures, especially at temperatures above 400 °C. Therefore, in order to obtain high coercivity at high temperatures, the Fe content in conventional Sm_2TM_{17}-type magnets has to be decreased. A high intrinsic coercivity of 0.66 MA/m at 400 °C was achieved when the Fe content was decreased from 15–20 wt.% in conventional Sm_2TM_{17} to 7 wt.%.

Sm also strongly affects the intrinsic coercivity at both room temperature and elevated temperatures. The intrinsic coercivity is very sensitive to the Sm content around room temperature. Generally speaking, increasing Sm content results in much lower room temperature coercivity but higher coercivity at high temperatures. With increasing Sm content, the sensitivity of coercivity to Sm content is gradually reduced and the coercivity peak tends to shift to the higher Sm content direction.

When dealing with the effect of Sm content (or z value) in $Sm(Co, Fe, Cu, Zr)_z$ magnets, it is important to realize that a small amount of Sm exists in the form of Sm_2O_3. Because Sm is a very active element, and some Sm is oxidized during the fine-powder processing. Under normal conditions, a sintered $Sm_2(Co, Fe, Cu, Zr)_{17}$-type magnet contains 0.3–0.6 wt.% oxygen. It is easy to understand that oxygen reduces the effective Sm content by 6.27 times the weight fraction of the oxygen. This means that for each 0.1 wt.% oxygen there will be 0.627 wt.% Sm to be consumed and reacted with oxygen. For this reason, every effort should be made to reduce oxygen pickup during processing.

It is well known that coercivity in the $Sm_2(Co, Fe, Cu, Zr)_{17}$-type magnets originates from the pinning of domain walls in the Cu-rich cell boundary phase in the fine-scaled cellular microstructure.[32,46] Therefore, sufficient Cu content is essential to develop high coercivity at both room temperature and high temperatures. Generally speaking, ${}_{\mathrm{M}}H_{\mathrm{c}}$ increases with the Cu content monotonously and increasing Cu content leads to higher coercivity at all temperatures.

Zr has an important effect on coercivity in the $Sm_2(Co, Fe, Cu, Zr)_{17}$-type magnets. It has been observed that Zr is critical in developing high coercivity at both low and high temperatures, especially for magnets containing a relatively higher Fe content. It was observed that intrinsic coercivity rapidly increased with increasing Zr and a peak coercivity value was reached at an optimum Zr content. The squareness of the 2nd-quadrant demagnetization curve is strongly dependent on the Zr content in magnet alloys. The knee field (the demagnetizing field corresponding to $0.9B_{\mathrm{r}}$) is rapidly enhanced with increasing Zr content. The effects of other transition metals, such as Ti, Hf, Nb, V, Ta, Cr, and Ni, on the high-temperature coercivity of $Sm_2(Co, Fe, Cu, Zr)_{17}$ were also investigated. All those elements decreased magnetization and only Nb demonstrated an effect of slightly enhancing coercivity at high temperatures.

6.2. New high-temperature $Sm_2(Co, Fe, Cu, Zr)_{17}$-type magnets

Based on systematic studies of the effects of compositions on high-temperature properties of $Sm_2(Co, Fe, Cu, Zr)_{17}$-type magnets, a new series of sintered permanent magnets with significantly improved high-temperature performance were ac-

complished by significantly reducing the Fe content, increasing the Sm content, and adjusting the Cu and Zr contents in magnet alloys. The maximum operating temperature of these magnets was increased from previous 300 °C for conventional high-temperature magnets to as high as 550 °C. The ${}_{\mathrm{M}}H_{\mathrm{c}}$ of these new magnets reached 1 MA/m at 400 °C (two to three times higher than those of conventional magnets) and 0.72 MA/m at 500 °C (four to nine times higher than those of conventional magnets). The B curves of these new magnets remained linear up to 550 °C (250 °C to 350 °C higher than those of conventional magnets). The temperature coefficients of ${}_{\mathrm{M}}H_{\mathrm{c}}$ for the new magnets can range from a small negative value (−0.03%/°C) to near zero, or they may even be positive (up to +0.3%/°C). As a comparison, the temperature coefficients of ${}_{\mathrm{M}}H_{\mathrm{c}}$ for conventional $SmCo_5$, Sm_2TM_{17}, and $Nd_2Fe_{14}B$-based magnets around room temperature are −0.3 %/°C, −0.3 %/°C, and −0.9 %/°C, respectively.

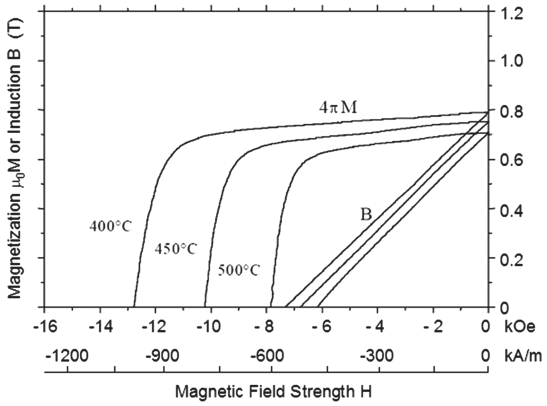


Fig. 16. Demagnetization curves of $Sm(Co_{0.79}Fe_{0.09}Cu_{0.09}Zr_{0.03})_{7.69}$ at 400 °C, 450 °C, and 500 °C.[47]

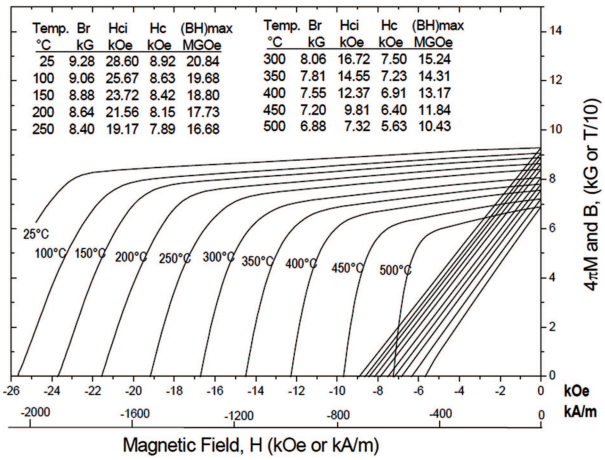


Fig. 17. Demagnetization curves of a new high-temperature magnet with $T_{\mathrm{max}} = 500$ °C.[48]

Figure 16 shows demagnetization curves of a $Sm(Co_{0.79}Fe_{0.09}Cu_{0.09}Zr_{0.03})_{7.69}$ at 400 °C, 450 °C, and 500 °C, respectively.[47] This magnet demonstrates much higher ${}_{\mathrm{M}}H_{\mathrm{c}}$ and better squareness of demagnetization curves at high temperatures than the conventional 2:17 magnets. Figure 17 shows demagnetization curves of a commercial new high-temperature magnet with its maximum operating temperature $T_{\mathrm{max}} = 500$ °C.[48] It can be seen from the figure that the room temperature $(BH)_{\mathrm{max}}$ of the magnet with $T_{\mathrm{max}} = 500$ °C is around 166 kJ/m^3. As a result of excessive amount of Sm, Cu, and Zr, the magnetization values of these new magnets are relatively low.

Figure 18 is a TEM micrograph of a new high-temperature magnet with $T_{\mathrm{max}} = 500$ °C. Comparing with that of the conventional 2:17 magnet (Fig. 9), the cellular structure has smaller cells and thicker cell boundaries.

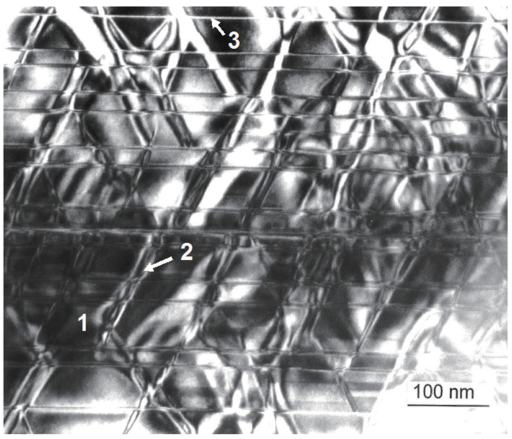


Fig. 18. TEM micrograph of a new high-temperature magnet with $T_{\mathrm{max}} = 500$ °C. 1: cell; 2: cell boundary; 3: platelet.[40]

6.3. Long-term thermal stability of new high-temperature permanent magnets

Figure 19 gives flux density loss versus time for a new magnet with $T_{\mathrm{max}} = 500$ °C and conventional 2:17 magnets with $(BH)_{\mathrm{max}} = 223$ kJ/m^3 and 234 kJ/m^3 (28 MGOe and 30 MGOe) during long-term aging at 500 °C in air. It can be seen from the figure that after aging for 2000 hours, the flux density loss was around 18%, 49%, and 69%, respectively.[49] The improvement of the new magnet is obvious.

The flux density loss is caused by three different mechanisms: (i) non-linear induction demagnetization curve (B curve); (ii) oxidation starting from the surface and gradually penetrating to the magnet interior; (iii) microstructure change, such as grain growth and phase transformation. The flux density loss caused by microstructure change is very limited, especially when the operating temperature is lower than 400 °C. When a magnet is operating at a temperature higher than its T_{M}, its non-linear B curve will result in a large irreversible flux density loss. This is the case for conventional 2:17 magnets shown in Fig. 19. On the other hand, the loss for the new magnet is caused primarily by the oxidation. Surface coating using Cr, W, or sulfamate Ni can significantly reduce the flux density loss caused by oxidation.[50] In addition, it was determined that $Sm_2(Co, Fe, Cu, Zr)_{17}$-type magnets demonstrated much better neutron radiation resistance as compared to Nd–Fe–B type magnets. It was noted that the radiation resistance

and thermal stability are somewhat related and the irradiation damage is most likely caused by a radiation-induced thermal effect. The excellent radiation resistance of 2:17 magnets was proved to be an advantage in space applications.[51]

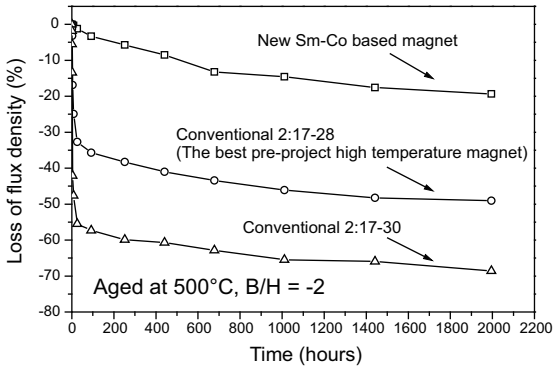


Fig. 19. Long-term thermal stability of a new-high temperature magnet with $T_{max} = 500$ °C.[49]

6.4. Abnormal temperature dependence of intrinsic coercivity

Novel temperature dependence of ${}_{M}H_c$ was observed during the research on high-temperature permanent magnets in some newly-developed magnets. A positive temperature coefficient of intrinsic coercivity in $SmTM_z$ with $z = 7$ was reported in 1998.[52] In 1999, a complex temperature coefficient in $Sm(Co_{0.843}Fe_{0.04}Cu_{0.09}Zr_{0.027})_{7.26}$ that had a low Fe content and a high Cu content was observed.[47] When heating this magnet, ${}_{M}H_c$ first gradually decreases and reaches a minimum at about 150 °C as shown in Fig. 20. With continued heating, ${}_{M}H_c$ rapidly increases and forms a maximum at 500 °C. The ${}_{M}H_c$ value of this magnet at 500 °C is more than 30% higher than its room temperature value. Another magnet of $Sm(Co_{0.825}Fe_{0.1}Cu_{0.05}Zr_{0.025})_{7.38}$ that has low Cu content displays a maximum ${}_{M}H_c$ at 550 °C, which is nearly four times higher than its room temperature coercivity value as shown in Fig. 21. The abnormal temperature dependence of coercivity in 2:17 magnets was observed by Russian researchers as early as in 1990.[53]

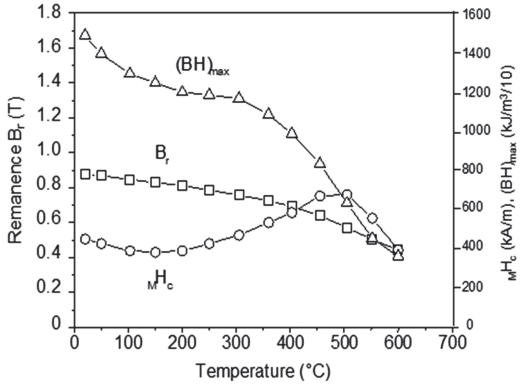


Fig. 20. Temperature dependence of magnetic properties of $Sm(Co_{0.843}Fe_{0.04}Cu_{0.09}Zr_{0.027})_{7.26}$.[47]

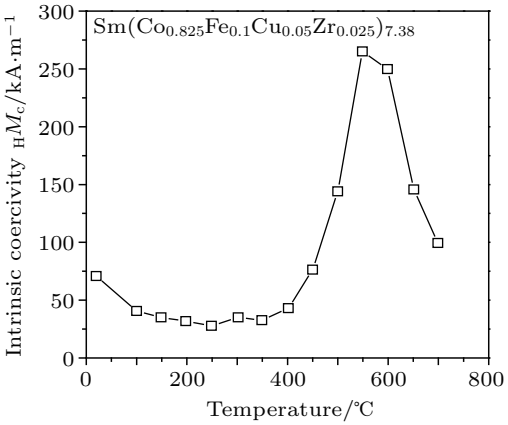


Fig. 21. Abnormal temperature dependence of coercivity for $Sm(Co_{0.825}Fe_{0.1}Cu_{0.05}Zr_{0.025})_{7.38}$.[53]

7. Thermal stability, temperature coefficient, and modeling of temperature-compensated magnets

7.1. Reversible and irreversible flux density loss

The open-circuit magnetic flux density loss caused by heating can be divided into two categories: (i) reversible loss, which can be recovered when the temperature returns to its original point; and (ii) irreversible loss. The irreversible loss can be further categorized into two types: 1) type I irreversible loss, which cannot be recovered even when the temperature returns to its original point, but can be recovered by re-magnetizing; 2) type II irreversible loss, which cannot be recovered even by re-magnetizing.

Normally, intrinsic coercivity decreases with increasing temperature. If a magnet remains its linear induction demagnetization curve at an elevated temperature, the open-circuit magnetic flux density loss is reversible. However, if at an elevated temperature, a knee appears on the induction demagnetization curve and the operating point of the magnet is close to the knee, then the magnetic flux density loss cannot be completely restored when the temperature returns to its original point, but the loss can be recovered by re-magnetizing. The type II irreversible loss cannot be restored even by re-magnetizing, because this type of loss is caused by microstructural changes, such as grain growth, phase transformation, and oxidation at elevated temperatures as mentioned previously.

It is obvious that approaches to improving the thermal stability of a magnet include (i) effectively increasing its intrinsic coercivity so that its induction demagnetization curve keeps linear at the operating temperature and (ii) protecting the magnet from oxidation and any structural changes.

7.2. Temperature coefficient

To describe the temperature dependence of a magnetic quantity, the temperature coefficient is often used and it is de-

fined as follows:

$$\alpha_{(T1\to T2)} = \frac{Q_{T2} - Q_{T1}}{Q_{T1}(T_2 - T_1)} \times 100 \ \ [\%/^\circ\mathrm{C}]. \tag{1}$$

where $\alpha_{(T1\to T2)}$ is the temperature coefficient of Q over the temperature interval from T_1 to T_2. However, $\alpha_{(T1\to T2)}$ is an average of temperature coefficients of Q over the temperature interval $T_1 \to T_2$, it is not necessarily an accurate description of the temperature dependence of Q, especially when the interval between T_1 and T_2 is large. Further, when Q is not a monotonous function of temperature T, equation (1) may give a misleading result.

On the other hand, the temperature coefficient of Q at a specific temperature T can be defined as

$$\alpha_{(\Delta T\to 0)} = \frac{\Delta Q}{Q\Delta T} \times 100 \ \ [\%/^\circ\mathrm{C}]. \tag{2}$$

When ΔT approaches 0, equation (2) leads to

$$\alpha_T = \frac{\mathrm{d}Q}{\mathrm{d}T}\frac{1}{Q} \times 100 \ \ [\%/^\circ\mathrm{C}]. \tag{3}$$

Obviously, α_T gives the temperature coefficient of Q at a specific temperature T. It is the true (or instantaneous) temperature coefficient and is a more accurate description of the temperature dependence of Q. Unfortunately, in practice, it is impossible to calculate α_T when $\Delta T = 0$ by simply using Eq. (2). This problem can be readily resolved if we use a polynomial to represent Q

$$Q(T) = a_0 + a_1 T + a_2 T^2 + \cdots + a_n T^n = \sum_{i=0}^{n} a_i T^i. \tag{4}$$

Coefficients a_0, a_1, a_2, and a_n in Eq. (4) can be determined using a least square fit, and it is very easy to determine the derivative of a polynomial. Therefore, we have

$$\frac{\mathrm{d}Q}{\mathrm{d}T} = a_1 + 2a_2 T + \cdots + n a_n T^{n-1} = \sum_{i=1}^{n} i a_i T^{i-1}. \tag{5}$$

Substituting Eqs. (4) and (5) in Eq. (3) yields

$$\alpha_T = \frac{\sum_{i=1}^{n} i a_i T_{i-1}}{\sum_{i=0}^{n} a_i T^i} \times 100 \ \ [\%/^\circ\mathrm{C}]. \tag{6}$$

Using Eq. (6), the true temperature coefficients a_T of any magnetic parameter Q at any temperature T can be readily determined and a plot of temperature coefficient versus temperature (α_T vs. T) can be drawn. Normally, since α_T is more sensitive to T than Q, the α_T vs. T plot is a very useful tool to represent the temperature characteristics of a magnetic parameter.

As an example, figure 22 shows the temperature dependence of magnetization at 0.8 MA/m for a sintered Gd_2(Co, Fe, Cu, Zr)$_{17}$ magnet. In the figure, the squares represent experimental data, while the curve is a 6$^{\text{th}}$ degree polynomial fit. In any experimental characterization, random errors are always associated with the results of measurements. The least square fit eliminates those random errors and, therefore, the numerical result is generally a better representation in comparison to the original experimental data. Figures 23–25 are plots of temperature coefficients of magnetization, intrinsic coercivity, and maximum energy product versus temperature for some sintered rare earth permanent magnets. This concept can be further developed for modeling of temperature coefficients of magnetization for temperature-compensated rare earth permanent magnets.

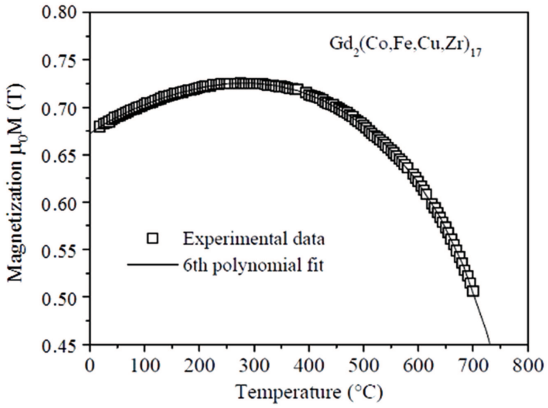


Fig. 22. Temperature dependence of magnetization at 0.8 MA/m of Gd_2(Co, Fe, Cu, Zr)$_{17}$.

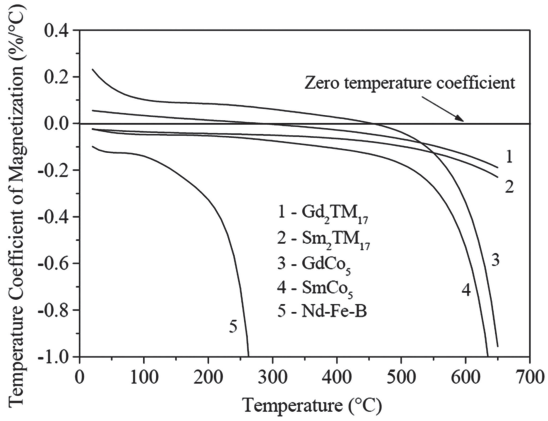


Fig. 23. Temperature coefficients of magnetization at 0.8 MA/m for some rare earth permanent magnets.

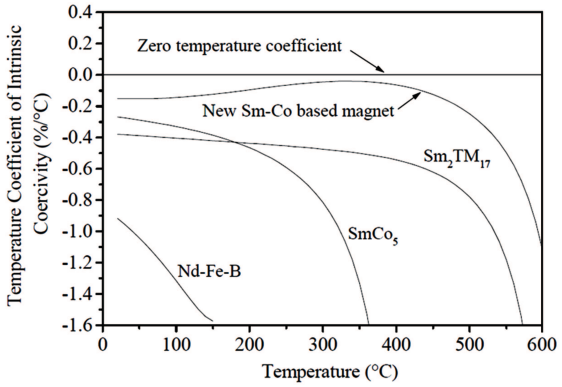


Fig. 24. Temperature coefficient of intrinsic coercivity for some rare earth permanent magnets.

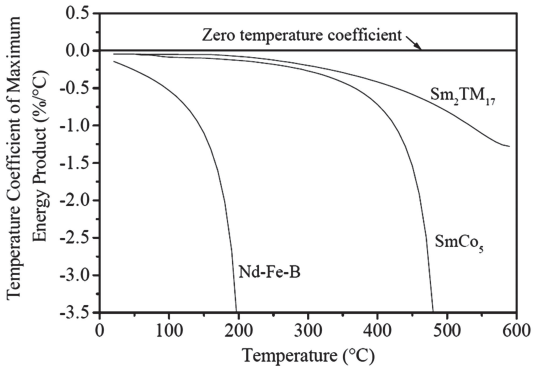


Fig. 25. Temperature coefficient of maximum energy product for some rare earth permanent magnets.

7.3. Modeling of temperature-compensated magnets

In addition to Gd, other heavy rare earths, such as Er and Ho, can also be used to make temperature-compensated magnets. Figure 26 compares temperature dependence of magnetization for a few heavy rare earth 2:17-type compounds. It can be seen from the figure that Er_2TM_{17} has the highest magnetization, while Ho_2TM_{17} has the highest T_p (temperature corresponding to the peak magnetization). Experiments indicated that Gd_2TM_{17} has high coercivity, while both Er_2TM_{17} and Ho_2TM_{17} showed low coercivity. Thus, it would be difficult to make a good temperature compensated magnet by using only one single heavy rare earth. To obtain a temperature-compensated permanent magnet with a high coercivity, a high magnetization, a high temperature for the peak magnetization, and a large temperature range for compensation, it seems Gd, Er, Ho, and probably more heavy rare earths, such as Tm, Yb, and Lu as previously mentioned, would have to be used. This typically requires considerable laboratory effort to determine the optimum combination of the light rare earth and the heavy rare earths. In research practice, a method of blending powders is often used. For example, by melting only two alloys of $SmCo_5$ and $GdCo_5$, any magnet alloys that have the composition of $(Sm_{1-x}Gd_x)Co_5$, with $0 \le x \le 1$ can be obtained by blending powders of $SmCo_5$ and $GdCo_5$.

Because saturation magnetization is an intrinsic property, it would be possible to calculate the temperature coefficient of saturation magnetization for a temperature-compensated *R*–TM magnet using a simple model, in which it is assumed that the magnetization of an $(LR_{1-x}HR_x)$–TM compound is independently contributed by LR–TM and HR–TM. As a first step of the modeling, the temperature dependence of saturation magnetization of, for example, $SmCo_5$ and $GdCo_5$ alloys should be experimentally determined by obtaining two functions $M_1(T)$ and $M_2(T)$. Then, two polynomials can be used to represent these two functions. Following that, these two polynomials can be "blended" (added) instead of two actual alloys, and resulting in a third polynomial

$$M_3(T) = (1-x)M_1(T) + xM_2(T), \tag{7}$$

where $0 \le x \le 1$. Next, the derivative of $M_3(T)$ with respect to T, $\mathrm{d}M_3(T)/\mathrm{d}T$ can be easily determined. Finally, the temperature coefficient of the new "alloy" at any specific temperature can be derived using

$$\alpha_T = \frac{\mathrm{d}M_3(T)}{\mathrm{d}T}\frac{1}{M_3(T)} \times 100 \ [\%/^\circ\mathrm{C}]. \tag{8}$$

In other words, the α_T vs. T relation for the new alloy can be readily established. Details of the numerical expression of this approach were given in Ref. [54] To demonstrate results of this modeling for temperature-compensated magnets, figures 27 and 28 give the calculated temperature dependence of magnetization for a few $(Sm,Gd)_2TM_{17}$, $(Sm,Ho)_2TM_{17}$, $(Sm,Er)_2TM_{17}$, $(Sm,Er,Ho)_2TM_{17}$, and $(Sm,Gd,Er,Ho)_2TM_{17}$ "magnets". While figures 29 and 30 show plots of the calculated temperature coefficients vs. temperature for some of these magnets.

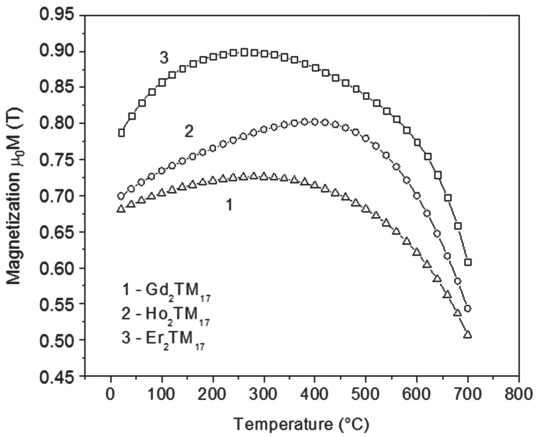


Fig. 26. Temperature dependence of magnetization for Gd_2TM_{17}, Ho_2Co_{17}, and Er_2Co_{17}.

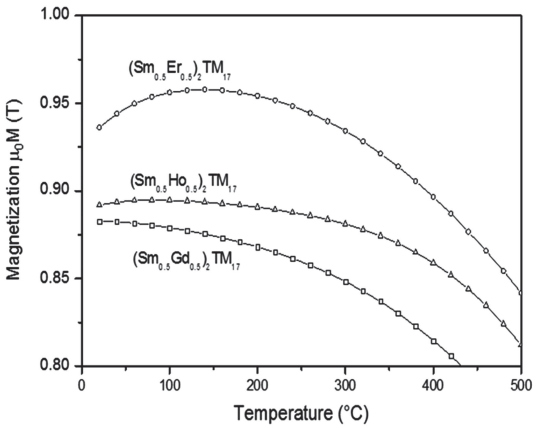


Fig. 27. Calculated temperature dependence of magnetization for $(Sm,Gd)_2TM_{17}$, $(Sm,Ho)_2TM_{17}$, and $(Sm,Er)_2TM_{17}$.

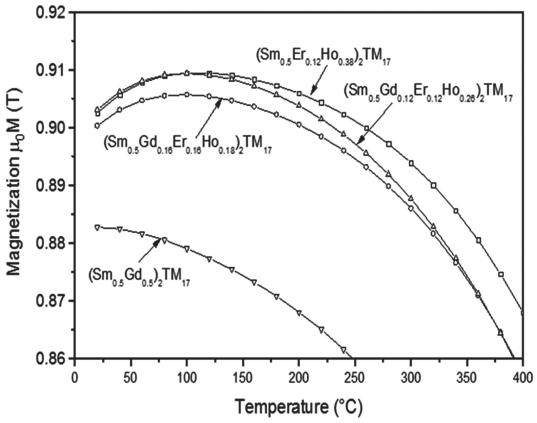


Fig. 28. Calculated temperature dependence of magnetization for $(Sm,Gd)_2TM_{17}$, $(Sm,Gd,Er,Ho)_2TM_{17}$, and $(Sm,Er,Ho)_2TM_{17}$.

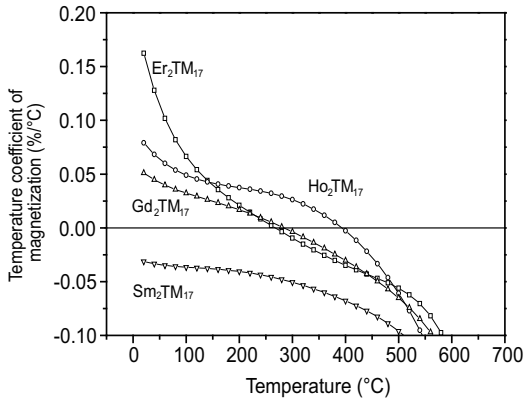


Fig. 29. A temperature coefficient of magnetization vs. temperature plot for Sm_2TM_{17}, Gd_2TM_{17}, Ho_2TM_{17}, and Er_2Co_{17}.

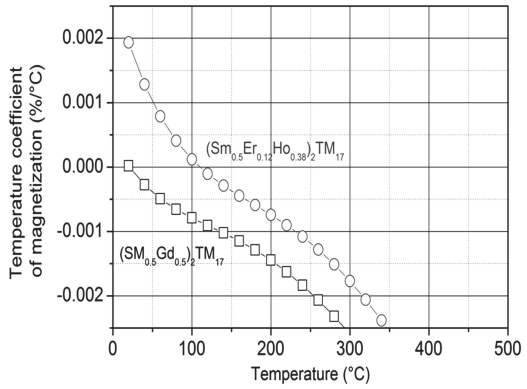


Fig. 30. A temperature coefficient of magnetization vs. temperature plot for temperature-compensated $(Sm,Gd)_2TM_{17}$ and $(Sm,Er,Ho)_2TM_{17}$.

8. Nanograin structure, nanocrystalline, and nanocomposite Sm–Co magnetic materials

High uniaxial magnetocrystalline anisotropy is a key prerequisite and a necessary condition for high coercivity in rare earth magnets; however, it is not the sufficient condition for high coercivity in conventional rare earth magnets with micrometer grain structure. A convincing example to illustrate this concept is the Sm_2Co_{17} compound. Though Sm_2Co_{17} has moderately high uniaxial magnetocrystalline anisotropy of 3.3 MJ/m^3, as mentioned previously, the coercivity of stoichiometric Sm_2Co_{17} is very low (usually less than 200 kA/m) if its grain size is in the micrometer range. In order to develop useful coercivity, extra Sm and considerable amounts ($\sim$ 10 at.%) of Cu and Zr must be added and a complex and time-consuming heat treatment procedure must be applied.[26–32] The procedure consists of high-temperature sintering at $\geq$ 1200 °C for 1–3 h, a solid solution heat treatment at $\sim$ 1180 °C for 2–4 h, and a long-term isothermal aging at $\sim$ 800 °C for 20–50 h. Even after this long-term isothermal aging, the coercivity is still very low. As demonstrated in Fig. 31, the high coercivity is developed after a very slow cooling from 800 °C to 400 °C at 1–2 °C/min followed by another isothermal aging at 400 °C for 10–20 h. The whole procedure takes about three days (up to 80 hours) to complete, as shown in Fig. 32. These compositional modification and long-term heat-treatment are required to form the specific fine-scale cellular microstructure in which the cell boundary phase serves as pinning sites for domain wall motion.

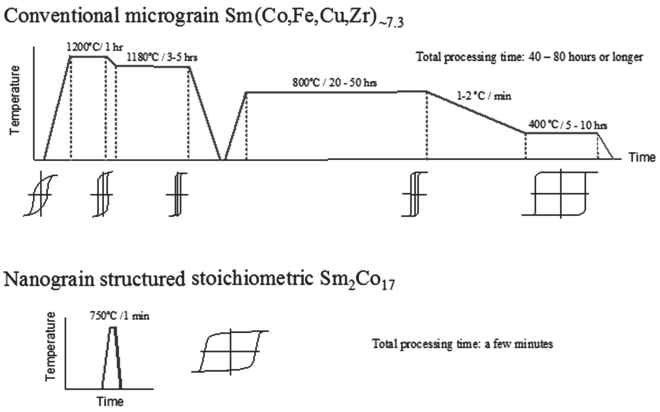


Fig. 31. Process and coercivity development comparison of conventional micrograin 2:17 (upper portion) and nanograin 2:17 magnet material[57] (lower portion).

However, if the grain size of Sm_2Co_{17} is reduced from micrometer range to nanometer range, high intrinsic coercivity can be easily developed in the stoichiometric Sm_2Co_{17} (without adding extra Sm and Cu, Zr and without long-term isothermal aging and slow cooling). In 1991, Wecker[55] obtained 0.5 MA/m after annealing a mechanically alloyed stoichiometric Sm_2Co_{17} alloy powder at 700 °C for 30 min. A few years later, Chen[56] obtained 0.3 MA/m after annealing a mechanically alloyed $SmCo_{10}$ alloy powder at 750 °C for 20 min. In 2003, a high coercivity of 1.24 MA/m was achieved after annealing a high-energy ball milled stoichiometric Sm_2Co_{17} specimen at 750 °C for only 1 min as shown in Fig. 32.[57] The TEM observation revealed nanograins of approximately 30 nm in average and no cellular structure was found as shown in Fig. 32. It should be noted that in order to achieve the similar level of coercivity, its micrograin counterpart must go through

a sintering, a solid solution heat treatment, and a long-term isothermal aging followed by a very slow cooling, totaling 80 hours, in addition to the Cu and Zr and extra Sm addition. Therefore, magnetization reversal in nanograin Sm_2Co_{17} must be carried out by a mechanism other than domain wall pinning.

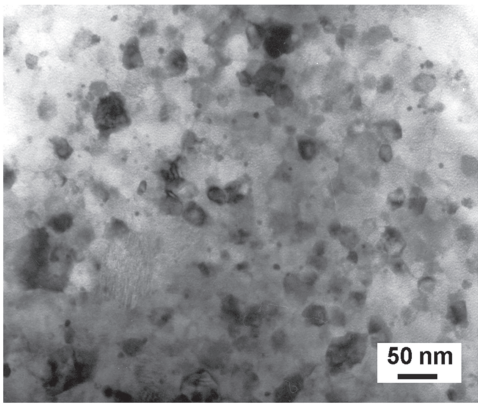


Fig. 32. TEM micrograph of a nanograin Sm_2Co_{17} magnet sample annealed at 750 °C for 1 min with ${}_{\rm M}H_{\rm c} = 1.24$ MA/m.[57]

Apparently, a fundamental change in coercivity mechanism takes place when the grain size of a rare earth magnet is reduced from the micrometer range to nanometer range. Based on novel phenomena observed in magnetic materials having nanograin structure, a new model of coercivity mechanism in magnetic materials with nanograins was proposed.[58,59] The principal points of this model are given as follows. (i) In magnetic materials with nanograins, the formation of multiple magnetic domains in a grain is no longer energetically favorable. (ii) The magnetization reversal in nanocrystalline and nanocomposite magnetic materials is not carried out by nucleation of reversed magnetic domains or domain wall motion, but by rotation of magnetization. (iii) Therefore, in magnetic materials with nanograin structure, there is no longer a need to create a specific microstructure to prevent the formation of reversed domains or to restrict domain wall motion. (iv) High uniaxial magnetocrystalline anisotropy is not only a necessary condition for high coercivity, as it is in magnetic materials with micrograins, it is also the sufficient condition for high coercivity in magnetic materials with nanograins. (v) Thus, a direct connection between coercivity and magnetocrystalline anisotropy is established in magnetic materials with nanograin structure. (vi) Consequently, high coercivity should be readily obtained for any magnetic materials that possess high uniaxial anisotropy, provided that the materials have nanograin structure. This concept can be schematically illustrated in Fig. 33.

To verify this concept experimentally, an YCo_5 alloy was chosen for a further test. YCo_5 was the first rare earth-transition metal compound that was discovered to have very high uniaxial magnetocrystalline anisotropy;[4] however, useful coercivity could not be obtained in a conventional material with micron grains. A high-energy ball milled YCo_5 powder was annealed at 750 °C for 2 min, and high coercivity near 1 MA/m was readily obtained in the first experiment.[93] Then, a moderately high coercivity of 0.6 MA/m was obtained after annealing a high-energy ball milled YCo_5/α-Fe (5 wt.%) at 750 °C for 2 min.[93] Figure 34 shows a TEM image and selected area electron diffraction pattern of the nanocomposite YCo_5/α-Fe specimen. The electron diffraction pattern demonstrates a mixture of a 1:5 structure and an α-Fe structure, while the TEM image is characterized with small α-Fe grains and twinned YCo_5 grains. In addition, the new coercivity concept has also been supported by experimental results obtained in Sm_2Co_{17}/Co, $(Sm,Gd)_2Co_{17}$/Co, and $Nd_2Fe_{14}B/\alpha$-Fe systems.

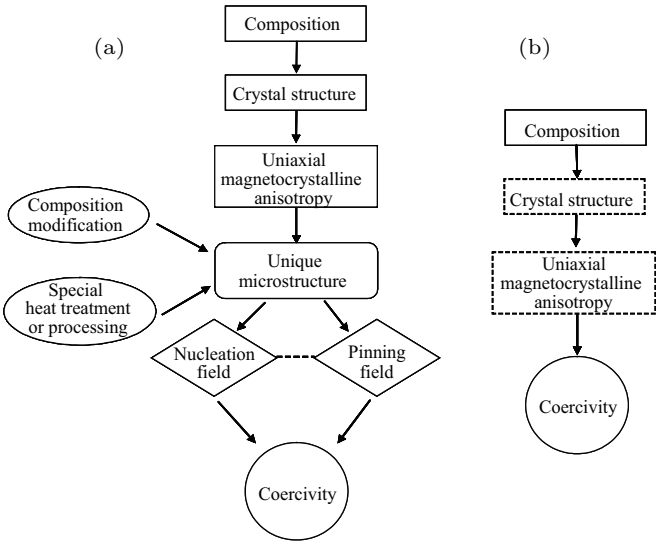


Fig. 33. Coercivity mechanisms in rare earth permanent magnets with micrograins (a), showing indirect connection between anisotropy and coercivity; and with nanograins (b), showing direct connection between anisotropy and coercivity.

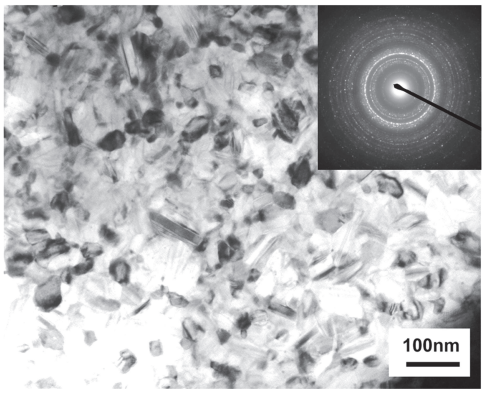


Fig. 34. TEM image and selected area electron diffraction pattern of a mechanically alloyed YCo_5/α-Fe specimen after annealing at 750 °C for 2 min.[93]

In a nanograin rare earth magnet material, the rare earth content can be reduced to lower than its chemical stoichiometric composition, resulting in a hard/soft nanocomposite magnet material. In nanocomposites, because of the hard/soft interface exchange coupling, the direction of magnetization in

the soft phase is restricted by that in the hard phase and tends to be aligned in the same direction as that in the hard phase. The exchange interaction of magnetic moments at the hard/soft interface is, in a way, like a spring, leading to the term exchange spring.

Getting rid of excessive Sm content and eliminating non-ferro-magnetic elements Cu and Zr from the conventional $Sm_2(Co, Fe, Cu, Zr)_{17}$-type magnets would significantly enhance magnetization and Curie temperature. Stoichiometric Sm_2Co_{17} possesses high saturation magnetization of 1.22 T and high Curie temperature of 917 °C. Partial substitute Fe for Co further increases the saturation magnetization of $Sm_2(Co_{0.7}Fe_{0.3})_{17}$ to 1.45 T. If nanocomposite $Sm_2(Co_{0.7}Fe_{0.3})_{17}$/Fe–Co could be made, its magnetization would reach the same level as $Nd_2Fe_{14}B$ (1.6 T) and it might be a new type of high-temperature and high-performance magnet, if sufficiently high coercivity could be developed.

However, there are multiple difficulties to accomplish this task. First, nanograin structures are created using rapid solidification, for example, melt spinning, and high-energy ball milling followed by crystallization. The products of these processes are ribbons or powders. Making these ribbons and powders fully dense materials without altering their nanostructure is a challenge. Second, near perfect grain alignment is necessary for any high-performance magnet materials. Aligning tiny nanograins, thus, forming anisotropic magnets is another challenge.

Melt spinning or high-energy ball milling followed by rapid hot compaction and hot deformation were successfully employed to make nanocomposite Nd–Fe–B/Fe or Nd–Fe–B/Fe–Co magnets by realizing fully dense bulk magnets and near perfect grain alignment. The hot compaction is not only a process for consolidation of powders or ribbons, but also a process for crystallization of amorphous materials. While in the followed hot deformation, the hot compacted bulk body is further made to near full density and the easy magnetization directions of all nanograins are aligned along the pressing direction.[58,59]

However, this approach has proved not very successful for making $Sm_2(Co, Fe)_{17}$/Fe–Co. Experiments demonstrated that only partial grain alignment could be established in $Sm_2(Co, Fe)_{17}$ and $Sm_2(Co, Fe)_{17}$/Fe–Co after hot compaction and hot deformation.[60,61] This may relate to the fact that there is no grain boundary Sm-rich phase in the Sm_2Co_{17}-based alloy systems, since it is well known that the grain boundary low-melting-point Nd-rich phase plays a critical role in grain alignment for Nd–Fe–B alloys during hot deformation.

Better results were obtained for hot deformed $SmCo_5$. Bulk, anisotropic, nanograin $SmCo_5$ magnets with coercivity of 795–3980 kA/m and $(BH)_{max}$ of 88–135 kJ/m^3 were synthesized by hot compacting the high-energy ball milled $SmCo_5$ powder at 700 °C, followed by hot deformation at 800–900 °C with a height reduction of 70%–90%.[62] Figure 35 shows a TEM micrograph of a hot-deformed bulk, anisotropic, nanocrystalline $SmCo_5$ specimen.[62]

Alternatively, surfactant-assisted high-energy ball milling was used to produce anisotropic $SmCo_5$ nanoflakes, and the subsequent magnetic alignment and compaction yielded bulk, anisotropic, nanocrystalline $SmCo_5$ magnets.[63–65] Figure 36 shows a SEM micrograph of anisotropic $SmCo_5$ nanoflakes.[64] In addition, many other processes, such as powder blending, powder particle coating, and magnetic field-assisted ball milling, were tested in recent years.

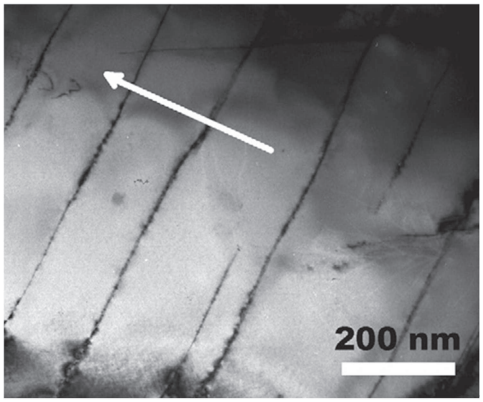


Fig. 35. TEM micrograph of hot deformed $SmCo_5$ with 90% height reduction.[62]

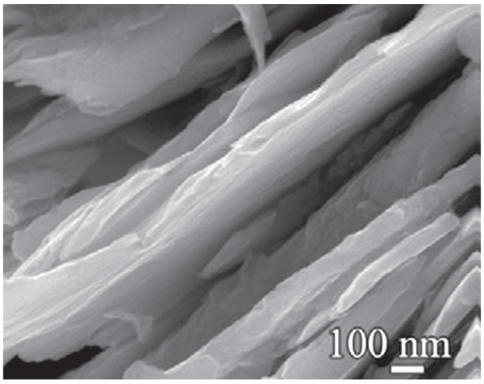


Fig. 36. SEM micrograph of anisotropic $SmCo_5$ flakes prepared by surfactant-assisted high-energy ball milling.[64]

It has been nearly 30 years since Buschow's group first reported magnetic properties in nanocomposite rare earth magnet materials.[66,67] However, these new type of materials, including both Sm–Co and Nd–Fe–B systems, remain in laboratory research stage, and their magnetic performance is still far poorer than that of their conventional counterparts. Technical difficulties in developing practical nanocomposite magnets include not only how to make bulk, fully dense, anisotropic magnets using adequate processes, but also how to develop sufficiently high intrinsic coercivity to ensure linear induction demagnetization curves.

Maintaining a linear induction demagnetization curve in a hard/soft nanocomposite magnet is a very difficult task. Introducing a soft magnetic phase, such as α-Fe or Fe–Co, will certainly enhance the magnetization, however, it will definitely result in reduced intrinsic coercivity, which will most likely lead to a non-linear B curve, as illustrated for curve 2 in Fig. 37. On the other hand, to remain a linear B curve, a magnet with higher magnetization needs to have higher intrinsic coercivity. This would lead to a contradictory dilemma: making a hard/soft two-phased nanocomposite magnet that possesses the intrinsic coercivity higher than a magnet without any soft phase, as shown for curve 3 in Fig. 37. If we consider applications at an elevated temperature, this task would be even more difficult to accomplish.

It seems a conclusion can be made that only when sufficient high intrinsic coercivity is successfully developed (in addition to full density and perfect grain alignment), then nanocomposite magnets would be in a position to compete with conventional Sm–Co and Nd–Fe–B magnets.

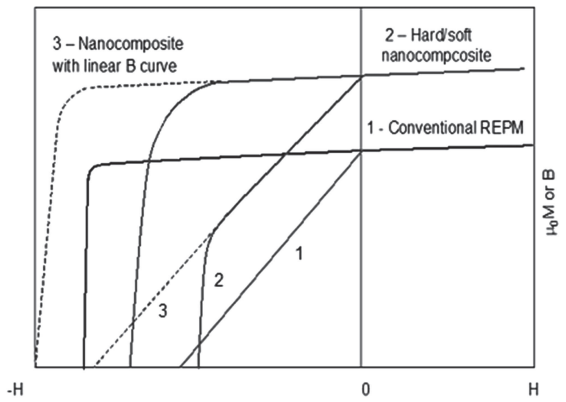


Fig. 37. Schematic illustration showing difficulty in developing hard/soft nanocomposite with a linear B curve.

9. Other Sm–Co permanent magnet materials

In addition to bulk magnets, Sm–Co thin films have been used in areas including, but not limiting to, microelectromechanical systems (MEMS) and magnetic recording. MEMS are miniaturized electromechanical devices, such as motors, actuators, sensors, mini-pumps, and micro-systems with coupled electric, mechanical, radiant, thermal, magnetic, and chemical effects. Some MEMS applications require a permanent magnet film up to a few hundred nanometers in thickness, while others use a permanent magnet 'thick layer' of a few microns, sometimes even to a few tenths of millimeters.[68]

Permanent magnets used for MEMS should have (i) proper coercivity, high remanence, high maximum energy product, and high Curie temperature; (ii) adequate to MEMS processing; and (iii) environmental stability, including mechanical stability, chemical stability, and thermal stability. Among all potential candidates, $SmCo_5$ thin film demonstrates the best magnetic performance; however, its corrosion resistance is poorer than that of some other materials, such as Pt–Co.[68]

On the other hand, the perpendicular magnetic recording can provide the storage density three times more than the traditional longitudinal recording. For the perpendicular recording, a thin film possessing high uniaxial anisotropy, with its c-axis perpendicular to the substrate surface, is required. This can be accomplished by epitaxially growing $SmCo_5$ thin film on an appropriate underlayer.[69]

Epitaxial $SmCo_5$ thin films with strong perpendicular magnetic anisotropy have been developed using sputtering or pulse laser deposition on various substrates, including Cu, Cu/Ti, W, Cr/Cu, Al_2O_3 (0001), heated Ru buffered Al_2O_3 (0001), Cr buffered single crystal MgO (110), and Ru/Cu/Ru sandwich, etc. and large perpendicular anisotropy and high coercivity have been achieved.[69–72]

In addition, it was reported that a high maximum energy product of 310 kJ/m^3 was achieved in a $SmCo_5$/Fe nanocomposite multilayer system,[94] which is higher than the theoretical value of the anisotropic single-phase $SmCo_5$ magnet (241 kJ/m^3).

10. Prospects of future rare earth permanent magnet materials

Three generations of rare earth magnets appeared around the mid-1960s, 1970s, and 1980s, respectively, which made people believe that we might have a new generation of rare earth magnets in about every ten years. However, 33 years have passed since the discovery of Nd–Fe–B magnets, there is still no sign of any new generation on the horizon. This fact made some pessimists even think that Nd–Fe–B might be the last high-performance rare earth permanent magnets.

In order to have reasonable prospects of future rare earth permanent magnet materials, we have to realize the distinguished differences between the developments of the 1st, 2nd generations and the 3rd generation rare earth magnets. It is obvious from Section 2 that the developments of $SmCo_5$- and Sm_2Co_{17}-based magnets were the outcome of systematic studies of binary R–Co compounds. When research on RCo_5 compounds started from the late 1950s, preliminary versions of R–Co phase diagrams were available and the existence of RCo_5 and some other R–Co compounds were already known.[73] Researcher's tasks, then, became to prepare R–Co intermetallic compounds and to test their basic magnetic parameters, including saturation magnetization values, Curie temperatures, and crystalline anisotropy fields, and to determine compounds that have potentials to be developed into practical permanent magnets.

The development of Nd–Fe–B magnets was very different from that of $SmCo_5$- and Sm_2Co_{17}-based magnets. To understand this important difference and its significance, it

is necessary to review the discovery of $Nd_2Fe_{14}B$ compound. In fact, searching candidates for permanent magnet materials was conducted simultaneously in both *R*–Co and *R*–Fe systems. Extensive investigation of *R*–Fe systems (R = Ce, Pr, Nd, Sm, Gd, Tb, Dy, Ho, Er, Tm, Lu, and Y) was carried out in the mid-1960s by Ray, Strnat, and their co-workers[74–77] at the US Wright-Patterson Air Force Base and the University of Dayton. Unfortunately, *R*–Fe binary compounds have neither high Curie temperature, nor uniaxial crystalline anisotropy, and therefore, did not appear promising.

In the 1970s, research on amorphous materials, including soft magnetic materials, using rapid solidification became very active and stimulated the hope for finding new metastable phases in *R*–Fe systems. In 1973, Clark[78] obtained an energy product of 69 kJ/m^3 by heating a $TbFe_2$ amorphous ribbon to 500 °C. Starting from 1980, Croat[79–82] studied melt-spun *R*–Fe-alloys (R = Pr, Nd, Sm, Gd, Tb, and Er) and obtained $(BH)_{max}$ = 24–32 kJ/m^3 in $Nd_{0.4}Fe_{0.6}$ and $Pr_{0.4}Fe_{0.6}$. Apparently, Koon[83,84] was the first person adding B to melt-spun *R*–Fe alloys. The purpose of adding B was to restrain the tendency of the melt-spun alloys to crystallize. Then, Hadjipanayis[85,86] also added Si and/or B into *R*–Fe systems to make it easier to obtain amorphous state during rapid quenching, as he mentioned that "the metalloid was included in the system to make the ribbons more glassy".[85] He also increased the Fe content to enhance the magnetization and obtained $(BH)_{max}$ = 103 kJ/m^3 in $Pr_{16}Fe_{76}B_5Si_3$ and $Pr_{16}Fe_{76}B_8$.

The fact that the x-ray diffraction spectrum of heat treated $Pr_{16}Fe_{76}B_5Si_3$ resembled that of a $Fe_{20}R_3B$ tetragnal phase discovered by Stadelmaier[87] caused Hadjipanayis to attribute the hard magnetic properties of $R_{16}Fe_{76}(B,Si)_8$ to this highly anisotropic phase. Since $R_3Fe_{20}B$ is a stable equilibrium phase, it was realized that the new *R*–Fe–B magnet might be made by traditional powder metallurgy method in addition to melt-spinning. Finally, in November 1983, Sagawa[88] in Japan reported that a $(BH)_{max}$ = 279 kJ/m^3 was obtained in $Nd_{15}Fe_{77}B_8$ using the same conventional powder metallurgy technique as that for producing $SmCo_5$, which symbolized the birth of the third generation of rare earth permanent magnets. Later studies revealed that the exact composition of the new compound is $R_2Fe_{14}B$, not $R_3Fe_{20}B$ as previously realized.

Apparently, the new $R_2Fe_{14}B$ compound was created in early 1980s without even its creator's (Koon and Hadjipanayis) recognition. The addition of B and/or Si into *R*–Fe was to make it easier to obtain an amorphous phase in a hope that new metastable phases could be formed in the heat treatment after rapid solidification. Therefore, the discovery of $Nd_2Fe_{14}B$ is a fortunate incidental or accidental event, or a lucky hit, rather than the outcome of systematic studies like what happened for $SmCo_5$ and Sm_2Co_{17}.

From the discovery of the $Nd_2Fe_{14}B$ compound, there are at least two lessons we can learn. The first lesson is that we must pay close attention to every incidental or accidental event in research. More often than not, the outcome of a research may be different from the original intention. This is not only true for $Nd_2Fe_{14}B$, but also true for the discovery of hard/soft nanocomposite rare earth magnetic materials.

When Buschow's group extended compositions of melt-spun *R*–Fe–B alloys to a more Fe-rich and B-rich range, their original intention was, again, to try to find metastable ferromagnetic materials for permanent magnets.[66] More Fe was added for a higher magnetization and more B was added for easier glass formation. But, the $R_2Fe_{23}B_3$ (R = Pr, Nd, Sm, and Gd) metastable ternary Fe-rich compounds they obtained all have cubic crystal structures and are not suitable for permanent magnet materials.

Later in 1989, after annealing amorphous melt spun flakes, they obtained a two-phased $Nd_2Fe_{14}B$ (15%)/Fe_3B (85%) nanocomposite magnet material with remarkable isotropic hard magnetic properties. The remanence $\mu_0 M_r$ is 1.2 T, intrinsic coercive fields $\mu_0 H_c$ is almost 0.4 T, and $(BH)_{max}$ = 95 kJ/m.[67] From that time on started the extensive research on nanocomposite rare earth permanent magnet materials. Therefore, the discovery of hard/soft two-phased nanocomposites is very similar to that of $Nd_2Fe_{14}B$ compounds.

It is obvious that $Nd_2Fe_{14}B$ is the first rare earth-transition metal compound with technical importance discovered in a ternary system. Since all binary *R*–Co and *R*–Fe systems have been thoroughly investigated, the chance of finding new promising equilibrium or metastable compounds in those systems is rare. The discovery of $Nd_2F_{14}B$ has opened up a new avenue for future research, which is to explore more ternary and multiple systems and it expands a vast new field of opportunities. It is reasonable to believe that $Nd_2Fe_{14}B$-based magnets are not the last high-performance rare earth magnets, but they are the first high-performance rare earth magnets in ternary and multiple systems. However, because of the greatly increased complexity in ternary and multiple systems, it will most likely take quite a long time before the next potential compound to emerge. We should not ignore the possibility that the next new high-performance magnet material would be discovered by another fortunate incidental event, like the case of $Nd_2Fe_{14}B$.

The second lesson we can learn from the discovery of the $Nd_2Fe_{14}B$ compound is that we must pay particular attention to the effect of atomic spacing on intrinsic magnetic properties. Nd_2Fe_{17} is the only stable compound in the binary Nd–Fe system. It has a rhombohedral crystal structure with a = 0.857 nm and c = 1.246 nm, unfavorable easy-basal-plane anisotropy, and unfavorable low Curie temperature of 57 °C.

By adding B, a new ternary $Nd_2Fe_{14}B$ compound forms. It has a tetragonal crystal structure with $a = 0.879$ nm, $c = 1.218$, uniaxial anisotropy with $H_a = 6$ MA/m, and Curie temperature of 312 °C. It is believed that these significant changes are originated from the atomic spacing variation.

In addition, when nitrogen or carbon was introduced into R_2Fe_{17} as interstitial atoms, the small increase of lattice constants yielded vast enhancement in magnetization, Curie temperature, and anisotropy field.[89,95] For example, comparing $Sm_2Fe_{17}N_3$ with Sm_2Fe_{17}, only about 2% increase in lattice constants was demonstrated, but 93% increase in Curie temperature (from 116 °C to 476 °C), 54% in saturation magnetization (from 1.0 T to 1.54 T) were observed, and the anisotropy changed from easy basal plane to uniaxial with $H_a = 11$ MA/m.

We simply cannot overemphasize the significance of atomic spacing, since according to the Bethe–Slater curve, the basic types of magnetization, such as paramagnetism, ferromagnetism, and antiferromagnetism, are closely related to atomic spacing. Altering atomic spacing through forming new compounds may result in a change of magnetic types. For example, Mn is antiferromagnetic below 100 K and paramagnetic at room temperature. However, Mn shows ferromagnetic in Mn–Al, Mn–Bi, Cu–Mn–Sn, and Cu–Mn–Al systems. If in the relatively distant future we are able to modify materials not only in micrometer and nanometer ranges, but also in an angstrom range by forming ternary or multiple system compounds, then it might be not impossible to change a material from paramagnetic or ferrimagnetic to ferromagnetic.

It is assumed that one of the future high-performance rare earth magnets might still take the form of R–T–M, where R is one or more rare earths that primarily contribute high crystalline anisotropy, and $R =$ Ce, Pr, Nd, Sm, Gd, Dy, Ho, or Er; T is one or more 3d (or 4d) transition metals that primarily contribute high Curie temperature and high magnetization, and $T =$ Co, Fe, Mn, Cr, or Mo, Nb; and M are one or more metals, or semi-metals, or non-metal elements, that are to adjust atomic spacing, and $M =$ Al, Si, Ga, Ge, etc.

11. Conclusions

In advanced power/propulsion systems for future aircraft, vehicles, and ships, permanent magnet materials capable of reliably operating at high temperatures up to ~ 450 °C are required. Those operating temperatures are far beyond the capability of Nd–Fe–B magnets.

Extensive research efforts performed around the year 2000 resulted in a new class of $Sm_2(Co, Fe, Cu, Zr)_{17}$-type magnets capable of operating at high temperatures up to 550 °C and these new magnets are commercially available in the market. However, as a result of excessive amount of Sm, Cu, and Zr, the magnetization values of these new magnets are relatively low.

When the grain size is reduced from micrometer to nanometer range, a direct connection between coercivity and magnetocrystalline anisotropy is established in magnetic materials. Consequently, high coercivity should be readily obtained for any magnetic materials that possess high uniaxial anisotropy, provided that the materials have nanograin structure. Therefore, it is possible to obtain high coercivity in stoichiometric Sm_2Co_{17} and $Sm_2(Co, Fe)_{17}$, and this was confirmed by experiments.

Getting rid of excessive Sm content and eliminating nonferro-magnetic elements Cu and Zr from the conventional $Sm_2(Co, Fe, Cu, Zr)_{17}$-type magnets would significantly enhance magnetization and Curie temperature. Obviously it is of great significance if nanocomposite $Sm_2(Co, Fe)_{17}$/Fe–Co with high magnetic performance could be made.

However, this effort has encountered many technical difficulties, including how to find appropriate processes to fabricate fully dense, anisotropic, nanocomposite magnets with perfect grain alignment. Obtaining sufficiently high intrinsic coercivity for maintaining a linear induction demagnetization curve in hard/soft nanocomposite magnets has proved to be very difficult. Only when sufficient high intrinsic coercivity is successfully developed (in addition to full density and perfect grain alignment), would nanocomposite magnets be in a position to compete with conventional Sm–Co and Nd–Fe–B magnets.

This paper gives a detailed historical review of the development of Sm–Co permanent magnets and this development is compared with that of $Nd_2Fe_{14}B$-based magnets. The developments of $SmCo_5$- and Sm_2Co_{17}-based magnets are the outcome of systematic studies, while the discovery of $Nd_2Fe_{14}B$ compound is quite different. The original purpose of adding boron into binary R–Fe ($R =$ La, Pr, and Nd) systems was to make it easier to obtain an amorphous phase in the hope of finding promising metastable binary phase. At the time researchers did not realized that they were actually creating a totally new ternary $Nd_2Fe_{14}B$ compound.

The discovery of $Nd_2F_{14}B$ has opened up a new avenue for future research, which is to exploring more ternary and multiple systems and it expands a vast new field of opportunities. In future research, more attention should be paid to the effects of atomic spacing on intrinsic magnetic properties. It is reasonable to believe that one of the future high-performance magnets might still take the form of R–T–M, where R is a rare earth that primarily contributes high crystalline anisotropy, T is a 3d transition metal that primarily contributes high Curie temperature and high magnetization, and M is another metal, or a semi-metal, or a non-metal element, that is added to form a new ternary compound and to adjust atomic spacing, just like

boron does in $Nd_2Fe_{14}B$.

Acknowledgment

The author would like to thank Mr. Y. Wang, Prof. D. T. Zhang, and Prof M. Yue of Beijing University of Technology, Prof. J. Edmondson of Michigan State University, Lucia Liu of Georgia Institute of Technology, and Prof. J. P. Liu of University of Texas at Arlington for their help in preparing this manuscript. Special gratitude goes to Yuhui Shen, my colleague at the University of Dayton Magnetics Laboratory, for her effort to search important references, correct errors in the manuscript, and useful discussions.

References

[1] Fingers R T and Rubertus C S 2000 *IEEE Trans. Magn.* **36** 3373
[2] Nesbitt E A, Wernick J H and Corenzwit E 1959 *J. Appl. Phys.* **30** 365
[3] Hubbard W M, Adams E and Gilfrich J Y 1960 *J. Appl. Phys.* **31** 368S
[4] Hoffer G and Strnat K 1966 *IEEE Trans. Magn.* **2** 487
[5] Strnat K J and Hoffer G 1965 *US Air Force Materials Lab. Technical Report* AFML-TR-65
[6] Strnat K, Hoffer G, Olson J, Ostertag W and Becker J J 1967 *J. Appl. Phys.* **38** 1001
[7] Strnat K, Oison J C and Hoffer G 1968 *J. Appl. Phys.* **39** 1263
[8] Nesbitt E A, Willens R C, Shrwood R C, Buehler E and Wernick J H 1968 *Appl. Phys. Letter* **12** 361
[9] Strnat K J, Hoffer G I, Olson J C and Kubach R W 1968 *IEEE Trans. Magn.* **4** 255
[10] Velge W A J J and Buschow K H J 1968 *J. Appl. Phys.* **39** 1717
[11] Becker J J 1968 *IEEE Trans. Magn.* **4** 239
[12] Buschow K H J, Luiten W, Naastepad P A and Westendorp F F 1968 *Philips Tech. Rev.* **29** 336
[13] Buschow K H J, Luiten W and Westendorp F F 1969 *J. Appl. Phys.* **40** 1309
[14] Das D K 1969 *IEEE Trans. Magn.* **5** 214
[15] Nesbitt E A, Chin G Y, Sherwood R C and Wernick J H 1969 *J. Appl. Phys.* **40** 4006
[16] Benz M G and Martin D L 1970 *Appl. Phys. Lett.* **17** 176
[17] Martin D L and Benz M G 1971 *Cobalt* **11** 50
[18] Strnat K, Hoffer G, Ostertag W and Olson J C 1966 *J. Appl. Phys.* **37** 1252
[19] Ray A E and Strnat K J 1971 *US Air Force Materials Lab. Technical Report* AFML-TR-71-53
[20] Ray A E and Strnat K J 1971 *US Air Force Materials Lab. Technical Report* AFML-TR-71-210
[21] Ray A E and Strnat K J 1972 *US Air Force Materials Lab. Technical Report* AFML-TR-72-99
[22] Ray A E and Strnat K J 1973 *US Air Force Materials Lab. Technical Report* AFML-TR-73-112
[23] Ray A E and Strnat K J 1973 *US Air Force Materials Lab. Technical Report* AFML-TR-73-276
[24] Ray A E and Strnat K J 1972 *Proc. 7th Rare Earth Metals Conf.*, A. A. Baikov Institute of Metals, Moscow, Russia, p. 75
[25] Mildrum H F, Hartings M S, Strnat K J and Tront J G 1973 *AIP Conf. Proc.* **10** 618
[26] Senno H and Tawara Y 1974 *IEEE Trans. Magn.* **10** 313
[27] Tawara Y and Senno H 1976 *Proc. 2nd Int'l Workshop on REPM,* Dayton, Ohio, USA, p. 340
[28] Nagel H 1976 *AIP Conf. Proc.* **29** 603
[29] Ojima T, Tomizawa S, Yoneyama T and Hori T 1977 *IEEE Trans. Magn.* **13** 1317
[30] Ojima T, Tomizawa S, Yoneyama T and Hori T 1977 *Jpn. J. Appl. Phys.* **16** 671
[31] Yoneyama T, Fukuno A and Ojima T 1979 *Proc. 4th Int'l Workshop on REPM,* Hakone, Japan, p. 407
[32] Mishra R K, Thomas G, Yoneyama T, Fukuno A and Ojima T 1981 *J. Appl. Phys.* **52** 2517
[33] Liu S and Ray A E 1989 *IEEE Trans. Magn.* **25** 3785
[34] Moffatt 1990 *Binary Alloy Phase Diagrams* (2nd Ed.) Vol. **2** p. 1241
[35] Khan Y 1974 *Proc. 11th Rare Earth Res. Conf.,* vol. II p. 652
[36] Buschow K H J and Goot A S van der 1968 *J. Less Common Met.* **14** 323
[37] Strnat K J 1988 *Rare Earth-Cobalt Permanent Magnets Ferromagnetic Mater.* (Elservier Science Publishers B. V.) Vol. **4** pp. 145–148, 154, 186, 195
[38] Skomski R and Coey J M D 1999 *Permanent Magnetism* (Bristol: Institute of Physics Publishing Ltd.) p. 136
[39] Poudyal N and Liu J P 2013 *J. Phys. D: Appl. Phys.* **46** 043001
[40] Fidler J, Schrefl T, Hoefinge S and Hajduga M 2004 *J. Phys.: Condens. Matter* **16** S455
[41] Narasimhan K S V L, Wallace W E and Hutchens R D 1974 *IEEE Trans. Magn.* **10** 729
[42] Narasimhan K S V L and Wallace W E 1977 *IEEE Trans. Magn.* **13** 1333
[43] Campbell P 1996 *Permanent Magnet Materials and Their Applications* (Cambridge: Cambridge University Press) p. 51
[44] Ray A E and Strnat K J 1972 *IEEE Trans. Magn.* **8** 516
[45] Ray A E 1984 *J. Appl. Phys.* **55** 2094
[46] Livingston J D and Martin D L 1977 *J. Appl. Phys.* **48** 2608
[47] Liu S, Yang J, Doyle G, Kuhl G E, Chen C, Walmer M S and Walmer M H 1999 *IEEE Trans. Magn.* **35** 3325
[48] Walmer M S, Chen C H, Walmer M H, Liu S and Kuhl E 2000 *Proc. 16th Int'l Workshop on REPM,* The Japan Institute of Metal, p. 41
[49] Liu S, Potts G, Doyle G, Yang J, Kuhl G E, Chen C, Walmer M S and Walmer M H 2000 *IEEE Trans. Magn.* **36** 3297
[50] Chen C H, Huang M Q, Foster J E, Monnette G, Middleton J, Higgins A and Liu S 2006 *Surf. & Coatings Techn.* **201** 3430
[51] Liu J, Vora P, Dent P, Walmer M, Chen C, Talnagi J, Wu S and Harmer M 2007 *Proc. Space Nucl. Conf.* p. 2036
[52] Liu J F, Chui T, Dimitrovv D and Hadjipanayis G C 1998 *Appl. Phys. Lett.* **73** 3007
[53] Popov A G, Korolev A V and Shchegoleva N N 1990 *Phys. Met. Mrtall.* **69** 100
[54] Liu S 2005 *Handbook of advanced Magnetic Materials* Vol. **4** (Beijing: Tsinghua University Press & Springer) p. 41
[55] Wecker J, Katter M and Schultz L 1991 *J. Appl. Phys.* **69** 6058
[56] Chen S K, Tsai J L and Chin T S 1996 *J. Appl. Phys.* **79** 5964
[57] Cui B Z, Huang M Q, Liu S 2003 *IEEE Trans. Magn.* **39** 2866
[58] Lee D, Hilton J S, Liu S, Zhang Y, Hadjipanayis G C and Chen C H 2003 *IEEE Trans. Magn.* **39** 2947
[59] Liu S, Lee D, Huang M Q, Higgins A, Shen Y, He Y and Chen C 2006 *Proc. 19th Int'l Workshop on REPM,* Beijing, China, p. 123
[60] Huang M Q, Turgut Z, Chen Z M, Shen Y H, Lee D, Higgins A, Chen C H, Liu S, Liu J F, Horwah J C and Fingers R T 2009 *J. Appl. Phys.* **105** 123915
[61] Gabay A M, Zhang Y and Hadjipanayis G C 2005 *J. Magn. Magn. Mater.* **294** 287
[62] Yue M, Zuo J H, Liu W Q, Lv W C, Zhang D T, Zhang J X, Guo Z H and Li W 2011 *J. Appl. Phys.* **109** 07A711
[63] Wang Y P, Li Y, Rong C B and Liu J P 2007 *Nanotechnology* **18** 465701
[64] Cui B Z, Li W F and Hadjipanayis G C 2011 *Acta Mater.* **59** 563
[65] Shen Y, Leontsev S O, Turgut Z, Lucas M S, Sheets A O and Horwath J C 2013 *IEEE Trans. Magn.* **49** 3244
[66] Buschow K H J, Dc D B and Coehoorn R 1988 *J. Less-Common Met.* **145** 601
[67] Coehoorn R, Mooij D B and de C 1989 *J. Magn. Magn. Matter* **80** 101
[68] Chin T 2000 *J. Magn. Magn. Mater.* **209** 75
[69] Morisako A, Kato I, Takei S and Liu X 2006 *J. Magn. Magn. Mater.* **303** e274
[70] Sayama J, Mizutani K, Asahi T, Ariake J and Ouchi K 2006 *J. Magn. Magn. Mater.* **301** 271

[71] Sayama J, Mizutani K, Asahi T and Osaka T 2004 *Appl. Phys. Lett.* **85** 5640

[72] Ohtakea M, Nukagaa Y, Kirinob F and Futamotoa M 2009 *J. Cryst. Growth* **311** 2251

[73] Hansen M and Anderko K 1958 *Constitution Binary Alloys* (New York: McGraw-Hill Book Company Inc.) p. 449

[74] Ray A E, Strnat K and Feldmann D 1963 *Proc.* 3*rd Conf. on RE Research,* Clearwater, FL, US, p. 443

[75] Strnat K, Hoffer G and Ray A E 1966 *IEEE Trans. Magn.* **2** 489

[76] Ray A E 1968 *Proc.* 7*rd Conf. on RE Research,* Coronado, CA, USA, **II** p. 473

[77] Strnat K J and Salmans L R 1968 *US Air Force Materials Lab. Technical Report* AFML-TR-68

[78] Clark A E 1973 *Appl. Phys. Lett.* **23** 642

[79] Croat J J 1980 *Appl. Phys. Lett.* **37** 1096

[80] Croat J J 1981 *Appl. Phys. Lett.* **39** 357

[81] Croat J J 1982 *J. Appl. Phys.* **53** 3161

[82] Croat J J 1982 *IEEE Trans. Magn.* **18** 1442

[83] Koon N C Williams C M and Das B N 1981 *J. Appl. Phys.* **52** 2535

[84] Koon N C and Das B N 1981 *Appl. Phys. Lett.* **39** 840

[85] Hadjipanayis G C, Hazelton R C and Lawless K R 1983 *Appl. Phys. Lett.* **43** 797

[86] Hadjipanayis G C, Hazelton R C and Lawless K R 1984 *J. Appl. Phys.* **55** 2073

[87] Stadelmaier H H and Park H K 1981 *Z. Metallkd.* **72** 417

[88] Sagawa M, Fujimura S, Togawa N, Yamamoto H and Matsuura Y 1984 *J. Appl. Phys.* **55** 2083

[89] Coey J M D and Hong S 1990 *J. Magn. Magn. Matter* **87** L251

[90] Miller A, D'Silva T and Rodringues H 1976 *IEEE Trans. Magn.* **12** 1006

[91] Liu S, Huang M Q, Shen Y, Higgins A, Lee D and He Y 2008 *Proc.* 20*th Int'l Workshop on REPM,* Knossos-Crete, Greece, p. 195

[92] Narasimhan K S V L 1976 *IEEE Trans. Magn.* **12** 1009

[93] Liu S and Lee D 2004 *Proc* 2004 *China Magnet Symposium* Xi'an, China, p. 77

[94] Sawatzki S, Heller R, Mickel Ch, Seifert M, Schultz L and Neu V 2011 *J. Appl. Phys.* **109** 123922

[95] Yang Y, Ge S, Zhang X, Kong L, Pan Q, Hou Y, Huang S and Yang L 1990 *Proc* 6*th Int'l Symposium on Anisotropy and Coercivity in RE-TM*, Pittsburgh, PA, USA, p. 190